UNIVERSITY OF CALIFORNIA

Los Angeles

Lubrication Models for Particle-Laden Thin Films

A dissertation submitted in partial satisfaction

of the requirements for the degree

Doctor of Philosophy in Mathematics

by

Benjamin Patrick Cook

2007

The dissertation of Benjamin Patrick Cook is approved.

_____

Pirouz Kavehpour

_____

Chris Anderson

_____

Russel Caflisch

_____

Andrea Bertozzi, Committee Chair

University of California, Los Angeles

2007

TABLE OF CONTENTS

List of Figures

ix

regarding this work, particularly the suggestion to study singular shocks.

Chapter 4 is a version of the manuscript Linear Stability of Particle-Laden Thin Films, by myself, Oleg Alexandrov, and Andrea Bertozzi, which is under review for publication in a special topics issue of the European Physics Journal.

Chapter 5 is a version of an unfinished single-author manuscript titled A Theory for Particle Settling and Shear-Induced Migration in Thin Film Flow that I am preparing to submit for publication. In this work, as in all the above research, I benefitted greatly from the advice and guidance of Professor Bertozzi.

Vita

1981	Born, Oak Lawn, Illinois, USA.
2003	B.S. (Physics and Mathematics), Duke University, Durham, North Carolina.
2004	M.A. (Mathematics), University of Calfornia, Los Angeles, California.

Publications

B. Cook, D. Marthaler, C. Topaz, A. Bertozzi, and M. Kemp. Fractional bandwidth reacquisition algorithms for VSW-MCM. In *Multi-Robot Systems: From Swarms to Intelligent Automata*, Volume II, 2003, Kluwer Academic Publishers, Dordrecht, A.C. Schultz et al. eds., pages 77-86.

B. P. Cook, H. O. Everitt, I. Avrutsky, A. Osinsky, A. Cai, J. F. Muth. Refractive indices of ZnSiN2 on r-plane sapphire. In *Applied Physics Letters* 86 (12), 2005, pages 121906-121908.

ABSTRACT OF THE DISSERTATION

Lubrication Models for Particle-Laden Thin Films

by

Benjamin Patrick Cook

Doctor of Philosophy in Mathematics

University of California, Los Angeles, 2007

Professor Andrea Bertozzi, Chair

We derive a lubrication model describing gravity-driven thin film flow of a suspension of heavy particles in viscous fluid. The main features of this continuum model are an effective mixture viscosity and a particle settling velocity, both depending on particle concentration. The resulting equations form a 2×2 system of conservation laws in the film thickness $h(x, t)$ and in ϕh, where $\phi(x, t)$ is the particle volume fraction. We study flows in one dimension under the constant flux boundary condition, which corresponds to the classical Riemann problem, and we find the system can have either double-shock or singular shock solutions. The double-shock solutions correspond to a particle-rich ridge that has been observed in such films. We present the details of both solutions and examine the effects of the particle settling model and of the microscopic length scale b at the contact line. The instability of the contact line is also examined through linear stability analysis, and it is found that the particle-rich ridge makes the contact line somewhat less unstable, while shifting the most unstable mode to a longer wavelength. A separate model is introduced which considers the balance between shear-induced migration and particle settling due to gravity. This model allows

the prediction of the qualitative features of the flow, i.e. whether particles accumulate in a ridge or settle to the substrate, in terms of the inclination angle α and bulk concentrations ϕ_0, and this prediction is compared with published experimental data.

CHAPTER 1

Introduction

The flow of thin films is important to many fields in science and engineering, such as the fluid lining of lungs, contact lenses, geophysical salinity currents, paint and other liquid coatings. From a fundamental perspective, thin films also provide an important experimental configuration for studying interfacial phenomena, such as capillarity, surface energy, and wetting. The mathematical and physical complexity of these phenomena has helped to motivate many theoretical, computational, and experimental studies of thin films. This literature is summarized in section 1.1.

Flows of complex materials such as mixtures are much less understood. Treating each particle in a large suspension explicitly is clearly undesirable, as the problem quickly becomes enormous as many microscopic variables are introduced. However continuum modeling of mixtures has proved challenging. The main components of such a model are phase segregation, and a large-scale constitutive description in terms of the phase composition. Both of these questions have been extensively explored by theoretical, computational, and experimental methods, resulting in several continuum models. These models are described in section 1.2.

Film flow of suspensions has received far less attention in the literature. In some sense it can be seen as a special case of suspension flow, and therefore represents an application with which to test the predictions of suspension models. However, the application of existing theories to film flows is not straightforward.

Film flows of Newtonian fluids have already proved to be a rich mathematical problem, and for particle-laden films one can expect all these complexities as well as others caused by material inhomogeneity.

This dissertation consists of three main results concerning particle-laden thin films. The remainder of this chapter is a summary of the relevant background material. Chapter 2 derives a model for particle-laden films similar to that introduced by Zhou et al. [ZDB05] and Zhou [Zho04]. In chapter 3 the shock solutions for this model are studied and some conclusions are drawn about the role of particle settling. A second result appearing in chapter 4, describing the contact line instability of such a film, was obtained through numerical simulations carried out by Oleg Alexandrov. This work uses a form of the equations that has been adapted to include horizontal particle diffusion. A third result, described in chapter 5, deals with the role of vertical particle diffusion in the selection among three qualitatively different settling behaviors that have been observed.

1.1 Thin Films

Before summarizing the literature of thin films, it is helpful to inspect the simplest model for film flow. In this case, the motion is determined simply by a balance between gravity and viscous stress. This can be seen by applying the standard lubrication approximation as follows. Consider a film on an inclined plane as in figure 1.1 with surface given by $z = h(x, y, t)$. Assuming a typical height H is much smaller than the length scale L in the plane on which the film varies, the Stokes equations in the plane are to leading order in H/L

$$\nabla p = \mu \frac{\partial^2 u}{\partial z^2} + (\rho g \sin \alpha) \hat{x}, \tag{1.1}$$
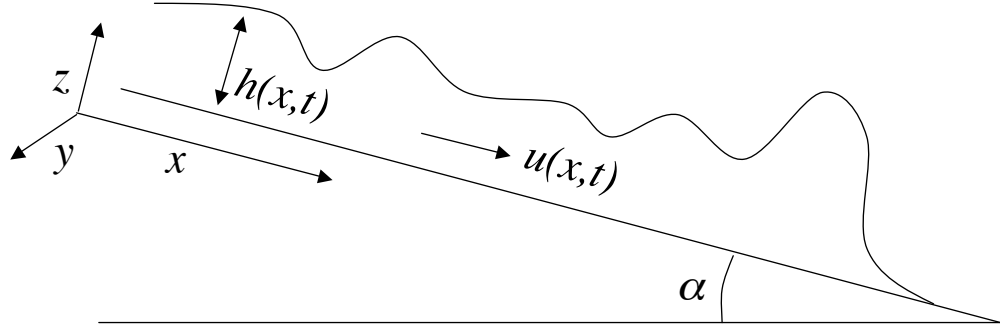
Figure 1.1: Geometry of the thin film.

where α is the angle the plane makes with the horizontal. The other assumption needed is that the variation of pressure with depth is simply hydrostatic, i.e.

$$p(z) = p(h) + (\rho g \cos \alpha)(h - z), \tag{1.2}$$

which ensures the fluid velocity is negligible in the z direction. The pressure at the free surface is specified as a boundary condition, it can be taken to be constant if surface tension is unimportant, otherwise it is given by the Laplace-Young condition

$$p\big(x, y, h(x, y)\big) = p_0 - \gamma \nabla^2 h(x, y) \tag{1.3}$$

with p_0 representing the atmospheric pressure. The second boundary condition is the no-slip condition at $z = 0$: $u(x, y, 0) = 0$. These conditions allow equation (1.1)) to be integrated vertically three times, resulting in the depth-averaged velocity

$$\bar{u} = \frac{h^2}{6\mu}\big[\gamma \nabla \nabla^2 h - (\rho g \cos \alpha) \nabla h + (\rho g \sin \alpha)\hat{x}\big]. \tag{1.4}$$

3

Equation (1.4) expresses the local balance of forces, and together with the in-compressibility condition it determines the evolution:

$$\frac{\partial h}{\partial t} + \nabla \cdot (h\bar{u}) = 0. \tag{1.5}$$

The lubrication approximation thus allows the Stokes equations for the three components of the fluid velocity, defined on an evolving three-dimensional domain, to be replaced with the single equation (1.5) for the film thickness on a fixed two-dimensional domain.

If both surface tension and the normal component of gravity are neglected, equation (1.5) reduces to

$$\frac{\partial h}{\partial t} + \frac{g \sin \alpha}{\nu} \frac{\partial}{\partial x} h^3 = 0. \tag{1.6}$$

Equation 1.6 was used by Huppert in 1982 as a basic model for film flow [Hup82]. It has the form of a conservation law, which can be solved by the method of characteristics. Huppert found in this way the solution for a finite volume of fluid, which is valid for t large enough that the initial distribution of fluid becomes unimportant. This solution is given by

$$h = \left(\frac{\nu}{g \sin \alpha} \frac{x}{t} \right)^{1/2} \tag{1.7}$$

for

$$0 \le x \le x_N = \left(\frac{9A^2 g \sin \alpha}{4\nu} t \right)^{1/3}, \tag{1.8}$$

and $h = 0$ for x out of this range. The discontinuity at $x = x_N$ is known as a shock, and the theory of such discontinuous solutions will be discussed in section (reference to cons. law section).

As suggested by Huppert, the discontinuity signifies a region where, since h varies on a shorter length scale, the lubrication approximation is less accurate

and forces such as capillarity become important. However, in experiments he reported in the same paper the front position was in good agreement with the values of x_N from the model, suggesting that a detailed understanding of the front region may not be necessary in order to describe the bulk flow.

Huppert also observed in these experiments that a planar film, after advancing for a time, becomes unstable at the front, and the interface forms a nearly periodic wavelike pattern. He compared the flows of two silicone oils with approximately the same surface tension and differing viscosity, and concluded the wavelength of the instability is independent of the fluid's viscosity. Comparing one of these with glycerine, with approximately the same viscosity and greater surface tension, he observed that glycerine displayed both a longer wavelength and a differently shaped instability: silicone oil resulted in an approximately triangular wave pattern, while glycerine formed a long thin finger-like shape.

Huppert also investigated the wavelength of the instability, and gave a scaling argument that the wavelength should be proportional to $(A^{1/2}\sigma/\rho g \sin\alpha)^{1/3}$, where A is the cross sectional area of the fluid. His experimental data was consistent with this scaling, and he was able to extract a proportionality constant of 7.5.

Huppert identifies two elements that are missing from this analysis: surface tension, and contact line effects. Modeling surface tension is straightforward, but contact lines, as the next section will show, present a greater challenge.

1.1.1 Contact Lines

Precisely, the contact line is the curve along which the solid, meets two separate fluids, typically air and a liquid. In an article in 1970, Huh and Scriven [HS71] provided the first full fluid dynamic treatment of the contact line problem. Ear-
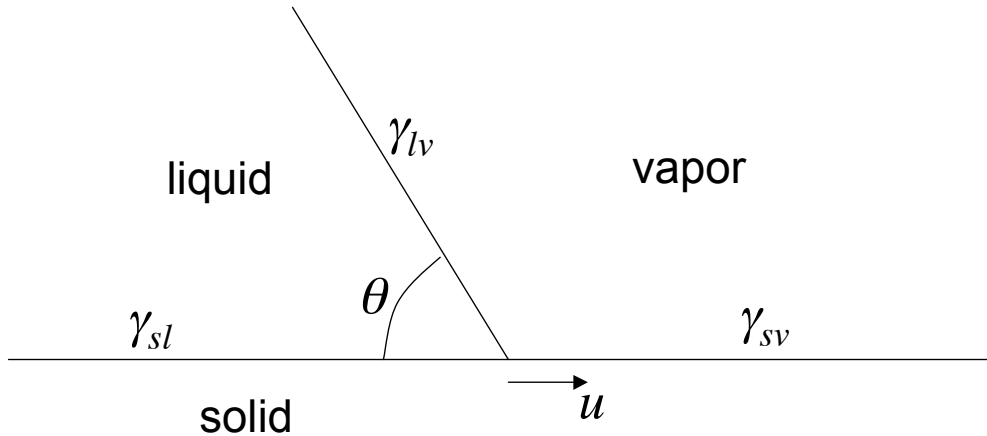
Figure 1.2: Geometry of the contact line.

lier studies by physical chemists, they noted, were concerned with measuring the contact angle (see figure 1.2). According to a simple thermodynamic argument, which assigns to the solid-vapor, solid-liquid, and liquid-vapor interfaces energies γ_{sv}, γ_{sl}, and γ_{lv} per unit area, a static contact angle θ at thermodynamic equilibrium must satisfy the Young-Dupré equation:

$$\gamma_{lv}\cos\theta + \gamma_{sl} = \gamma_{sv}, \tag{1.9}$$

which minimizes the total interfacial energy [You05]. However this equation was not verifiable, since accurate measurements of solid surface energies were not yet available. Measurements of the contact angle itself lacked reproducibility as well, due to an effect known as contact angle hysteresis: θ takes larger values when the fluid is advancing (or has recently advanced), smaller values when it is receding (or has recently receded), and there exists a range of stable angles at which a contact line may remain stationary. They also point out that the contact angle can depend on the level of magnification at which it is measured, and in some

6

circumstances a microscopic film can develop beyond the apparent location of the contact line.

Nonetheless, the contact angle appears to be an essential parameter in describing the geometry of contact line motion. In their model, Huh and Scriven assumed a constant contact line speed, a constant contact angle, and chose all interfaces to be planar. With these assumptions, they solved the Stokes equations for Newtonian fluids in both fluid domains, subject to the following boundary conditions: equality of the fluid and solid velocities at the fluid-solid interfaces, and continuity of the fluid velocity and tangential stress across the fluid-fluid interface. These conditions are sufficient to determine a single solution, and Huh and Scriven present a closed-form expression for this solution in terms of the contact angle and the relative viscosities of the two fluids. The velocity, however, is undefined at the contact line itself, and they also point out that this solution implies an infinite force exerted by the fluid on the solid. The conclude that the model cannot therefore be valid, and claim the no-slip boundary condition at the fluid-solid interfaces, manifested in the matching of the tangential fluid velocity to that of the solid, is responsible for this paradox.

In 1974 Dussan V. and Davis extended this fluid dynamical treatment of the contact line problem. They analyzed the singularity under more general conditions, without any assumptions about the constitutive behavior of the fluids and solid, the shape or energy properties of the interface, or 2-dimensionality of the flow. Their basic assumption was that the either points on the fluid-fluid interface are mapped onto the contact line by the evolution, or vice versa, i.e. the forward or the backward streak line emanating from the contact line coincides with the fluid-fluid interface. They also worked with a generalized no-slip condition, in order to deal with discontinuous velocities, that states that a

fluid element can come in contact with at most one point on the solid boundary for all time, without requiring the element to remain on the boundary after contact is made. They then proved that the opposite (backward or forward) streak line lies in the interior of one fluid domain, while the other fluid displays what they described as a "rolling" motion. They also performed experiments with dyed fluids that demonstrated precisely this flow pattern.

Furthermore, they showed that under these conditions the velocity must be multi-valued at the contact line, and for Newtonian fluids the force exerted on the solid must be infinite. Thus the paradox is significantly more general than the case studied by Huh and Scriven. Both Huh and Scriven and Dussan V. and Davis point out that a modified boundary condition at the solid interface allowing some degree of slip would alleviate the singularity. Dussan V. and Davis also suggest that the fluid may also become non-Newtonian near the contact line, and since the singularity is logarithmic in the distance from the contact line, this effect may only be needed at extremely short length scales.

Much progress has been made since these early papers, though a summary of the entire field is beyond the scope of this introduction. The problem from the fluid mechanics perspective, of choosing appropriate boundary conditions for the Stokes equations, remains complex, and practical models are typically not derived from first principles. A 1985 review article by de Gennes [de 85] describes how the above paradoxes have been explained. Contact angle hysteresis has been attributed to imperfections in the solid, which tend to "pin" the contact line at defect locations.

The energy paradox is best understood in the case of "completely wetting" materials, in which the spreading energy

$$S = \gamma_{SV} - \gamma_{SL} - \gamma_{LV} \tag{1.10}$$

8

is positive. The subscripts S, L, and V refer to the solid, liquid, and vapor phases. It is then energetically favorable for the film to coat the entire surface, so long as this layer is thick enough that continuum theory, and hence the bulk surface energies, make sense. An equilibrium thickness is determined by van der Waals forces, long-range intermolecular forces, between the liquid and solid. Near a moving contact line, a film will transition from a wedge shape with a small positive contact angle, such as studied by Huh and Scriven and Dussan V. and Davis, to a nearly flat precursor film, at approximately this equilibrium thickness. Typical precursor thicknesses are on the order of 10 nanometers. Finally, the true contact line at the tip of the precursor will avoid the singularity described by Dussan V. and Davis, because the slowly thinning precursor will ultimately reach a length scale at which continuum models break down. (Individual molecules, of course, can slip.) The considerable energy dissipated in the viscous stress of the the precursor flow is supplied by van der Waals forces, which are a manifestation of the energy S released by spreading.

Polymer liquids, including the silicone oils that are popular with experimentalists due to their readily controlled viscosity, also display significant slip at the solid boundary. Slip models are commonly expressed by a mixed boundary condition for the tangential velocity u_t of the form

$$u_t = b \frac{\partial u_t}{\partial \nu}, \tag{1.11}$$

where ν is a coordinate normal to the boundary and b is a modeling parameter. This can be interpreted as letting the linear extrapolation of the velocity vanish at a distance b past the boundary, and b is therefore known as the slip length or extrapolation length. Experiments by Léger et al. [LHM97] find slip lengths of 1 micrometer and higher for silicone oils. The effect is thought to be caused by the straightening near the boundary of the molecular chains, which in bulk

9

flow are highly tangled, contributing to the material's high viscosity. As noted by both Huh and Scriven and by Dussan V. and Davis, a slip boundary condition removes the stress singularity at a contact line. Thus both slip and the precursor film are equally accurate explanations of the energy paradox for polymer liquids. As discussed in the following section, models for moving contact lines commonly include one but not both of these effects, introducing the minimum amount of complexity needed to avoid a stress singularity.

1.1.2 Advancing Films

An early model for a film problem involving an advancing contact line was introduced by Greenspan in 1977 [Gre78]. He considers the one-dimensional spreading on a horizontal surface of both an axisymmetric drop and a planar sheet similar to that of Huppert. This model incorporates a slip length $\beta = \alpha/3h$, with α of the order 10^{-10}cm^2, thus slip becomes significant only near the contact line. Assuming surface tension, rather than gravity, is the dominant driving force, Greenspan derives the equation

$$\frac{\partial h}{\partial t} + \frac{\sigma}{3\mu}\nabla \cdot \left[h(h^2 + \alpha)\nabla\nabla^2 h\right] = 0 \qquad (1.12)$$

for the film thickness $h(x, y, t)$. Specifying the slip in the interior of the fluid domain does not provide a boundary condition at the contact line, so he also requires the normal velocity of the boundary is proportional to the deviation of the dynamic contact angle $\theta = \arctan|\nabla h|$ from its static value θ_s, motivated by published experimental data for the case $|\theta - \theta_s| \ll \theta_s \ll 1$. He then finds that leading order solutions for small values of a modified capillary number $\epsilon = 3\mu\kappa/\theta^2\sigma$ have constant curvature, so axisymmetric drops take the form of a spherical cap. The nondimensional radius $a(t)$ evolves by

$$\dot{a}(t) = 1/a^3 - 1, \qquad (1.13)$$

relaxing to the equilibrium radius $a = 1$. The completely wetting situation corresponds to the limit $a \ll 1$, and the solutions scale as $(t+c)^{1/4}$ with c depending on the initial data. The corresponding one-dimensional problem describes a straight ridge spreading into a planar film. The equation becomes

$$\dot{a} = 1/a^2 - 1, \tag{1.14}$$

so that a scales like $(t + c)^{1/3}$ for completely wetting films. This is the same time scaling that Huppert found for the gravity-driven film on an incline, even though both the driving forces and the shape of the film differ.

A study by Silvi and Dussan V [SD85] probed the instability observed by Huppert, by distinguishing between surface tension and contact line effects. They repeated the Huppert experiment using a single fluid, glycerin, and two surfaces made of glass and Plexiglas, so that any differences can be attributed to the contact line physics and not to surface tension. They found the same two instability patterns, the sawtooth pattern occurring on glass and the fingering pattern occurring on Plexiglas. Comparing their results with those of Huppert, they concluded that the fingering patter occurs when the contact angle is large, including glycerin on both plastic surfaces, and the sawtooth pattern occurs for small contact angles, including glycerin on glass and silicone oil on Perspex. Their results were also consistent with Huppert's relation between the surface tension coefficient and the wavelength of the instability, suggesting that surface tension is the initial cause of both instabilities.

A subsequent paper by Schwartz analyzes the same problem numerically. The simulations begin with a mound of fluid $h(x, y)$, which evolves by the lubrication equation

$$h_t = \nabla \cdot \left[h^3 (\cos \alpha \nabla h - B^{-1} \nabla \nabla^2 h - \mathbf{i} \sin \alpha) \right], \tag{1.15}$$

where $B = \rho g L^2 / \sigma$ is a Bond number and L is a characteristic length scale. The

11

equation is solved in conservation form, and boundary cells are given a nonzero flux only from adjacent interior cells, in order to model a no-slip condition at the side wall. This flux does however permit the contact line to advance at the boundary. This equation does not include slip, nor did Schwartz explicitly introduce a model for the contact line, rather he simply solved the equation at every cell with $h = 0$ for dry regions, which he suggests is appropriate for a completely wetting flow.

The resulting numerical solutions show a saw-tooth instability pattern similar to that which Silvi and Dussan V linked to completely wetting experiments. Schwartz observed this instability growing both from the perturbation imposed by the side wall, and in simulations with an imposed perturbation and no wall, indicating that is was not merely a wall effect. He further showed that the instability requires surface tension: a series of simulations with $B^{-1} = 0$ failed to develop any instability.

Troian et al. studied the contact line instability of a vertical film by posing a matched asymptotic problem [THS89]. For the y-independent base state they began with Huppert's solution for the region away from the contact line (outer region), and defined a quasi-steady inner region where surface tension is significant. They posed an asymptotic problem for an inner solution $h(\xi)$ such that the film height is given by $H(x, y, t) = H_N(t)h(\xi, t)$. The inner solution scales as $H_N(t)$, the nose height from the outer solution, and the inner length scale is given by $l = H_N(3Ca)^{1/3}$ in terms of the capillary number $Ca = (\mu/\sigma)dX_N/dt$. The matching condition with the outer solution is that $h(\infty) = 0$, and they relieved the stress singularity at the contact line by matching to a precursor film of thickness bH_N. The equation they derived for the inner region,

$$h^2(1 - h_{\xi\xi\xi}) = \frac{1 - b^3}{1 - b} - (1 + b)\frac{b}{h}, \qquad (1.16)$$

was solved numerically, and solutions were found to have a pronounced hump that depends weakly (logarithmically) on the value of b. There are also weak oscillations as the hump decays to the outer value of 1. Thus their model requires the parameter b that is not known a priori, though an estimate of the order of magnitude may be sufficient for many purposes.

They next studied the linear stability of periodic perturbations in the y direction. The looked at two-dimensional solutions for which the contact line structure is displaced a distance $\xi_B(\zeta, t) = -A(\zeta)B(t)$ from the base state $\xi = 0$, where $\zeta = y/l$ is the scaled y coordinate. Assuming a sinusoidal form for A, they calculated the linearized growth rate for the amplitude $B \ll 1$, and found that the perturbations grow at long wavelengths. They also calculated the most unstable wavelength to be about $14l$, which is fairly close to the value $18l$ they estimated from Huppert's data.

It was noted by Schwartz, Troian et al, and others that the hump that appears behind the contact line seems to be associated with the onset of instability. Motivated by this insight, Goodwin and Homsy [GH91] to studied the hump in more detail. They derived a first model for this region by the principle that specifying a contact angle will supply the needed information regarding the physics of the contact line, eliminating the need for any unknown parameters. Working under the assumption of small contact angles ϕ and small capillary number $Ca = U\mu/\gamma$, they considered the limit $\tan\phi \to 0$, $(\tan^3\phi)/Ca \to 1$, and scaled the problem accordingly so that the contact angle boundary condition becomes $h_x = -1$ at $x = 0$. They also incorporated slip at the solid boundary $y = 0$ of the form

$$3u = S(h)u_y - \left(1 + S(h)\right) \tag{1.17}$$

for an unspecified function S, where y is the coordinate normal to the plane. Applying the lubrication approximation, they find that the surface satisfies the

equation

$$h_{xxx} = \frac{1 + S(h)}{S(h)h + h^2} - 1. \tag{1.18}$$

By choosing $S(h) = O(h^{-1})$ as $h \to 0$ they find the stress singularity is removed, similar to the analysis of Greenspan. However, the derivative of the curvature is infinite at the contact line, which under the lubrication approximation implies infinite fluid velocities, and they conclude that the lubrication approximation is therefore inappropriate for this region.

Goodwin and Homsy note that the failure of the lubrication approximation can be expected as the horizontal and vertical length scales become comparable, which happens near the contact line for finite contact angles. Therefore they introduce a Stokes flow problem for a region near the contact line in which both x and y are scaled as $h_N(t)$, the height determined from the outer region by Huppert's calculation. Using a boundary integral numerical method, they were able to solve for the quasi-steady Stokes flow in a moving reference frame following the contact line, and report the results of simulations for a wide range of ϕ, Ca, and inclination angle α. In the fixed volume experiment conducted by Huppert, the capillary number of the hump region decreases with time, corresponding in Goodwin and Homsy's results to a growing hump relative to the surrounding film. This is consistent with the hypothesis that a large hump, with its associated high curvature, is responsible for the instability.

An experimental study by Jerrett and de Bruyn [Jd92] investigated the speed of the film front before and after the onset of instability. They found the front position before the instability was well described by a power law function of time, however they observed exponents significantly greater than the value 1/3 predicted by Huppert: about 1/2 for heavy mineral oil (HMO) and 2/3 for glycerin on Plexiglas. Data for very small inclination angles ($\alpha \lesssim 5°$) suggests that this

anomalously large exponent is a transient that eventually slows to 1/3. They note that Huppert's theory is valid for long enough times that the initial conditions do not matter, and infer from the larger exponent that the initial conditions are still relevant for their experiment.

Once the instability appeared they observed a finger-shaped pattern for both fluids. The unstable front was described in terms of the positions of finger tips and troughs as a function of time, with the tips continuing to move at a power law rate with approximately the same exponent as the stable film, and the troughs moving at a linear rate after an exponential transient. Since experimental flows are well beyond the range of linear perturbations, they find there is no theory with which to compare the fingering results. A heuristic discussion, though, suggests that the sawtooth shape results from both small contact angles (as predicted by Silvi and Dussan V) and weak dependence of the advancing contact angle on the advancing velocity, while the fingering pattern is associated with the opposite properties.

Subsequently de Bruyn [de 92] performed the same experiment with silicone oil on glass, for which the sawtooth pattern appears. He measured the amplitude of the pattern as a function of time, and found it was not well described by the exponential growth characteristic of linear instability. While the vertical flow condition $(3Ca)^{1/3} \ll \tan \alpha$ used by Troian et al. was not satisfied by de Bruyn's experiment, he was able to meaningfully compare his results with their theory. Guided by Troian et al.'s scaling, de Bruyn plotted finger length versus time, scaled by the capillary length l and l/U, where U is the velocity of the contact line, and found the data for eight values of α between 2° and 21° collapsed toward a single curve. From the rescaled data it was also apparent that the fingers grow exponentially until a dimensionless time of approximately 40, and

was independent of α. The measured growth rate β was approximately 0.11, compared with the 0.5 in Troian et al.'s calculations. However, these calculations are valid for α much larger than in the experiment, so quantitative agreement is not to be expected.

Spaid and Homsy [SH95] then reconsidered the linear stability analysis of Troian et al. They used two contact line models, a precursor and a slip model, and found for both the base state and the instability problem that the both models give very similar results when the precursor thickness is equated with the slip length. They also determine from the stability calculations that unlike the Rayleigh instability in which surface tension causes a cylindrical jet to break up in to drops when breakup results in smaller total surface area, the fingering instability is driven by gravity, which causes thicker regions of the film to flow faster, and surface tension is a stabilizing force. They also consider a perturbation representing a weakly viscoelastic fluid, and find viscoelasticity to also be a stabilizing effect.

Bertozzi and Brenner [BB97] repeated the linear stability analysis for the precursor model while retaining the terms for gravity normal to the plane, which had been neglected by Troian et al., thereby extending the result to arbitrary α. The equation is expressed

$$h_t + (h^3)_x + \nabla \cdot \left(h^3 \nabla \nabla^2 h - D(\alpha) h^3 \nabla h \right) = 0, \qquad (1.19)$$

where $D(\alpha) = (3Ca)^{1/3} \cot \alpha$, so that the work of Goodwin and Homsy corresponds to the limit $Ca \to 0$, $D(\alpha) = 1$. This reflects the fact that both surface tension and the normal component of gravity act to smooth the profile near the contact line, in the form of nonlinear fouth- and second-order diffusion respectively. The bump occurs for small values of D, when the fourth-order term dominates, while at large values of D the smoothed profile is monotone. They find

that the contact line is linearly unstable to long-wave perturbations only when D is small enough to induce a bump in the profile, corresponding to $\alpha \gtrsim 5 - 10°$. This implies that for the smaller angles used by de Bruyn the films were linearly stable, even though the fingering pattern was observed. Bertozzi and Brenner explain this discrepancy in a discussion of transient growth. They find in the linearized problem that a small perturbation can grow by a factor on the order of $1/b$ before its ultimate exponential decay, where bh_N is the precursor thickness. Since reasonable sizes for the precursor may be on the order of a micron, corresponding to $b = 10^{-3} - 10^{-4}$, this amplification can be large indeed, and certainly large enough to engage nonlinear growth mechanisms, which they conclude are responsible for the observed instability at low angles.

Veretennikov, Indeikina, and Chang [IVC98] have observed thicker films, finding a different flow pattern near the contact line that they describe as a "nose front." This flow is characterized by a contact angle greater than 90° and a recirculating vortex structure, such that fluid simply falls down onto the solid ahead of the contact line, essentially creating a new contact line kinematically faster than the existing line can advance by thermal processes. Recall that Dussan V. and Davis described the two fluids (liquid and air) at a moving contact line taking two flow patterns, a rolling motion and a unidirectional wedge motion, and it is the latter that suffers a stress singularity under no-slip conditions. In this context, a nose front corresponds to the liquid assuming the rolling role, and therefore the no-slip condition is not problematic. They performed experiments on both dry and pre-wet surfaces, and found the nose flow to be more common on dry surfaces. They found an instability in nose fronts similar to that observed for thinner wedge fronts, and the shape of the fingers depends on the existence and thickness of a pre-wetted film on the surface. They suggest that the instability for nose fronts occurs when the film becomes too thin to support the nose

flow across the whole width, and the first areas to transition to wedge flow move slower to become troughs in the fingering pattern.

Kalliadasis [Kal00] carried out a nonlinear analysis of the fingering instability under the precursor model, retaining terms up to third order in the amplitude of the perturbation. Using center manifold theory, he arrived at a Kuramoto-Sivashinsky-type equation for the dominant mode describing the displacement of the contact line. Numerical solutions of this equation indicate a sawtooth shape for the fingering pattern similar to that observed in experiments, and the wavelength of the pattern was found to be sensitive to the precursor thickness. Since parallel-sided fingers were never observed, Kalliadasis concludes that the precursor model is inappropriate for dry spreading at large contact angles.

Eres, Schwartz, and Roy [ESR00], in order to more accurately describe partially-wetting films, introduced another term into the lubrication equation that explicitly models the van der Waals forces at the contact line. This model states that the pressure at the free surface is given by the sum of the standard capillary pressure term and a disjoining pressure given by $B[(b/h)^3 - (b/h)^2]$. This pressure is minimized when $h = b$, which causes a precursor layer of depth b to form, and is nearly constant when $h \gg b$. The coefficient B is equal to $\sigma\theta_e^2/b$ for a static contact angle θ_e. In numerical solutions of the resulting equation, they found three different fingering behaviors. The first two correspond to the well-documented sawtooth and parallel-sided fingering patterns at small and moderately large θ_e. They found that the sawtooth pattern grows to a maximum amplitude and then simply translates downstream, while the finger-shaped pattern grows apparently without bound. At still larger θ_e, they found parallel-sided fingers grow and ultimately break up into drops.

Bertozzi, Munch, and Shearer [BMS99] studied a related advancing film prob-

lem in which a film is driven up a vertical surface by a heat-induced gradient of the surface tension coefficient, motivated by an experiment performed by Ludviksson and Lightfoot [LL71]. After rescaling the variables, the equation takes the form

$$h_t + (h^2 - h^3)_x = -(h^3 h_{xxx})_x \qquad (1.20)$$

where the h^2 and h^3 terms represent the Marangoni and gravitation forces, respectively, and the fourth-order term represents surface tension. They seek solutions with weak curvature, so that the equation is interpreted as a conservation law with the non-convex flux $(h^2 - h^3)$ and the fourth-order term acts as a mild regularization. Ludviksson and Lightfoot had solved the unregularized problem for travelling waves connecting a constant downstream thickness h_∞ to a precursor b upstream. For certain realistic values of h_∞ and b the unique entropy solution consists of a rarefaction and a shock, however that solution was not observed in the experiment. Bertozzi et al. analyzed the effect of the regularizing term, and discovered that this solution may not occur in the regularized problem. They found another solution that is robust under this regularization, consisting of a rarefaction and an undercompressive shock which travels at a different speed than the entropy shock and separates from the rarefaction. They demonstrated the existence of a regularized solution using dynamical systems theory and presented numerical solutions of the regularized equation that approach the undercompressive shock solution. They also found that the undercompressive shock solution is consistent with Ludviksson and Lightfoot's qualitative descriptions of their experimental results.

Further simulations by Kondic and Diez [KD01] of using the precursor model predict that both sawtooth and finger-shaped patterns can occur in a completely wetting film. They find that the sawtooth pattern occurs at smaller α and the

finger-shaped pattern occurs at larger α. They also study the long-time evolution of these patterns, and like Eres et al. they find the sawtooth pattern saturates at a maximum amplitude, at which point it appears to settle into a stable traveling wave profile. Both patterns were observed to ultimately cover the whole plane. They also find that in a small area in front of the apparent contact line, the film thickness is less than the precursor. Fluid in this region actually moves upstream briefly due to the negative capillary pressure, until it is incorporated into the thicker forward-moving film.

1.2 Suspension Flow

1.2.1 Viscosity

The natural starting point for a suspension flow model is to describe the mixture as a simple fluid with modified physical properties, since the mass and momentum densities can be simply obtained by adding the density for each phase. The other crucial property that must be included is the viscosity. For simplicity it is most common to describe the mixture as effectively Newtonian, in which case the viscosity is a scalar, but unknown, function of concentration. However more complex behavior does exist, and can include shear thinning, shear thickening, and yield stresses [Sat95].

Einstein [Ein06] may have been the first analyze theoretically the viscosity of a mixture. Considering a dilute suspension of spheres, he derived the expression $\mu_r = 1 + 5\phi/2 + O(\phi^2)$ for the relative viscosity $\mu_r = \mu/\mu_f$ which is just the mixture viscosity scaled by that of the suspending fluid μ_f, and ϕ is the volume fraction of the spheres. The coefficient of the ϕ^2 term in the expansion was calculated to be 7.6 ± 0.8 by Batchelor and Green [BG72] for pure shear flows, and sensitive

20

to the bulk flow in general. This dependence is very complex, since the stress depends on the spatial arrangement of the particles, which in turn depends on the large scale flow.

Due to this complexity, empirical functions are generally used to describe the relative viscosity. These functions generally satisfy $\mu_r(0) = 1$, $\mu'_r(0) = 5/2$, and $\lim_{\phi \to \phi_m} \mu_r(\phi) = \infty$, although the second condition is sometimes violated. ϕ_m represents the maximum permissible concentration corresponding to close packing, and a range of values have been used from the simple cubic value 0.524 to the hexagonal packing value 0.740. One of the most common viscosity functions was first used by Krieger [Kri72]:

$$\mu_r(\phi) = \left(1 - \frac{\phi}{\phi_m}\right)^{-5\phi_m/2}. \tag{1.21}$$

Other viscosity functions are somewhat similar to equation 1.21 and generally diverge with an exponent of about -2. Simulations of suspensions have also been carried out by solving the Stokes equations subject to no-slip boundary conditions on the surface of each particle. One of the most common methods is Stokesian dynamics [BB88, SB01], which has been used to simulate as many as a few thousand particles. Both simulations and experiments become difficult for ϕ above $0.5 - 0.6$, however, as particles contact each other and form clusters or chains that can prevent steady shearing. This phenomenon is sometimes described as a phase transition, and the highly concentrated state has been compared to a crystal or a glass.

1.2.2 Settling

Suspensions of non-neutrally buoyant particles do not behave macroscopically as a single fluid, of course, because gravity tends to segregate the particles from the

fluid. For particles smaller than a micron or so, this effect can be reversed by electrical repulsion due to surface charges and/or Brownian motion of the particles, producing a colloidal suspension that remains mixed indefinitely, however this dissertation is concerned with larger non-Brownian particles for which buoyancy is relevant.

Scaling dictates that the average settling velocity be expressed as

$$v_s(\phi) = f(\phi) \frac{2a^2(\rho_s - \rho)g}{9\mu},$$ (1.22)

where the right hand side is the product of an unknown hindered settling function f with the exact settling velocity for a single sphere of radius a and density ρ_s in an unbounded fluid. It should be expected that $f(0) = 1$, since in an infinitely dilute suspension particles separated enough to not affect each other's motion. That the hindered settling function decreases with ϕ can be seen by considering that the liquid must also move past the particles, and the corresponding viscous dissipation increases as the separation between particles becomes small. In practice this decreased settling rate is observable for ϕ as low as 0.01.

Assuming such a form for the settling rate, i.e. one that is local in space and decreasing in ϕ, leads in finite systems to a kinematic shock structure that was described by Kynch [Kyn52]. The rescaled settling problem can be written as the conservation law

$$\phi_t - \left(\phi f(\phi)\right)_z = 0,$$ (1.23)

which in one dimension has solutions consisting of two shocks moving down from the top of the vessel and up from the bottom, which separate a top region void of particles, a center region at the initial (uniform) concentration, and a packed bed at the bottom. The shock speeds are given by the Rankine-Hugoniot jump condition (see chapter 3) expressing mass continuity, which determines the top shock moves with speed $-f(\phi_0)$ and the bottom with speed $f(\phi_0)\phi_0/(\phi_m - \phi_0)$

for initial uniform concentration ϕ_0. Thus the value of $f(\phi_0)$ can be measured by simply observing the speed of the top shock.

A review of many experiments aimed at determining the hindered settling function, both of the kinematic shock type described above and fluidization experiments in which particles remain stationary amidst a vertical flow of liquid, has been conducted by Barnea and Mizrahi [BM73]. They found that among several candidate functions, the best fit was achieved by the formula

$$f(\phi) = \frac{(1-\phi)^2}{(1+\phi^{1/3})\exp\left(5\phi/(1-\phi)\right)}. \tag{1.24}$$

The function $f(\phi) = (1-\phi)^n$, proposed by Richardson and Zaki [RZ54], has been more popular in the literature however, probably due to its simpler form. A study by Garside and Al-Dibouni [GA77] found that the best fit in this case is obtained at $n = 5.1$. It is interesting to note that both functions vanish not at ϕ_m but at $\phi = 1$, indicating that a packed configuration of particles that cannot shear can nevertheless be penetrated by a fluid current. While the experimental interpretation of this point in general is unclear, it turns out to be important in the thin film model and will be discussed in section 3.4.

Particle settling is a complex theoretical problem, including many of the same difficulties as the effective viscosity problem, and is a subject of ongoing research. Because of the complexity of the theoretical settling problem, empirical results such as those above are commonly used for modeling sedimenting mixtures. Low concentration limits have been studied, typically by solving for fluid velocities in a representative cell containing a single particle, which leads to the formula $f(\phi) = 1 - \beta\phi^{1/3}$. However, the value of β depends on the details of the shape of the unit cell and ad hoc boundary assumptions, so even at small concentrations the relevance of this type of model is questionable.

These representative cell calculations show that, like the viscosity, the sedi-

mentation velocity depends on the configuration of the particles. Thus the dilute result of Batchelor [Bat72] for a random fixed array is open to the same criticism. Furthermore, Caflisch and Luke [CL85] showed in 1985 that for such a system the velocity fluctuations about the mean $\langle \delta V^2 \rangle$ scale as $V_0^2 \phi L/a$, where V_0 is the single particle settling velocity and L is the size of the container. For sufficiently large systems, therefore, the fluctuations are so large that the mean velocity becomes meaningless.

1.2.3 Shear-Induced Migration

It was first observed in 1986 by Leighton and Acrivos [LA87] that if a suspension is sheared in a bob-in-cup Couette device, particles would slowly migrate out of the sheared gap into the adjacent reservoir, eventually causing a measurably lower concentration and viscosity in the gap. They found their experiments were consistent with a shear-induced diffusion process, with the diffusion coefficient proportional to $a^2 \dot{\gamma}$, where $\dot{\gamma}$ is the shear rate. They also found in the same experiment a short time increase in the measured viscosity, consistent with a related diffusion process whereby the concentration equilibrates across the gap, after an initial inhomogeneity resulting from the loading process. In terms of the simple shear geometry of the Couette experiment, the observations can be expressed as: 1) a flux of particles normal to the plane of shear, opposite a gradient in the shear rate, and 2) a flux of particles in the direction of shear (perpendicular to the velocity), opposite a gradient in concentration.

Leighton and Acrivos introduce three particle-scale effects in a model to account for the measured net fluxes in terms of statistical particle encounters. Since their experiments occurred at fairly high concentrations, they focused on irreversible interactions arising from forces of contact between particles. This is in
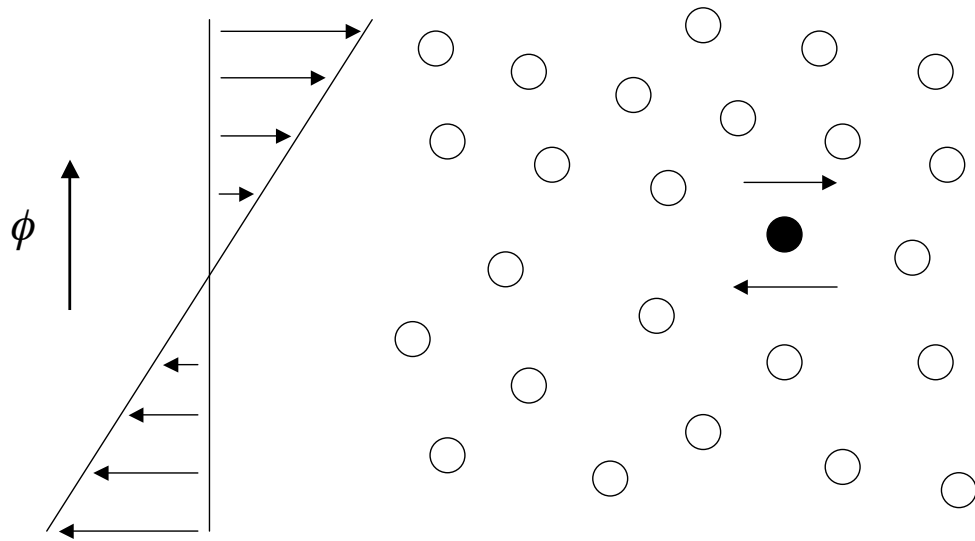
Figure 1.3: Influence of concentration gradients on shear-induced migration. Particles experiencing higher concentrations will interact more frequently, resulting in a diffusive flux.
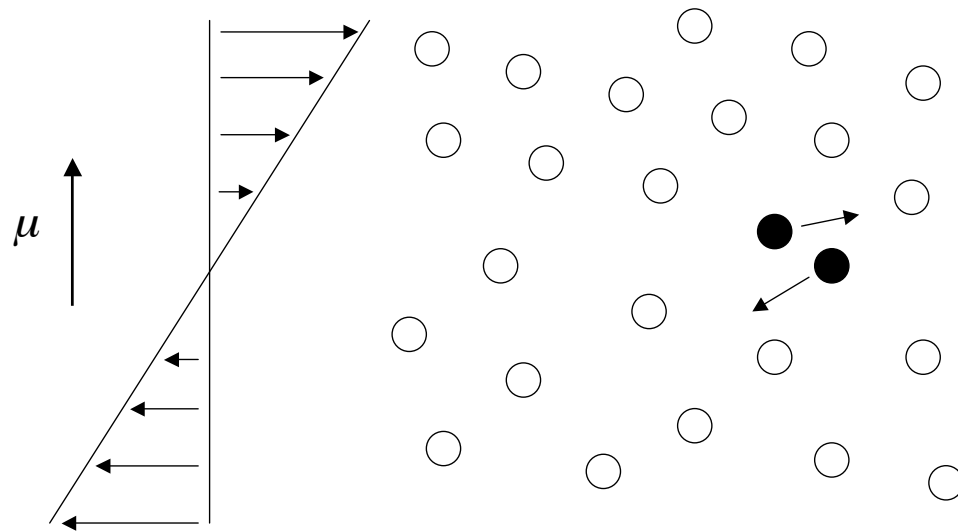
Figure 1.4: Influence of the local viscosity on the asymmetric interactions leading to shear-induced migration. The particle experiencing a smaller local viscosity is displaced farther, causing a net flux opposite the viscosity gradient.
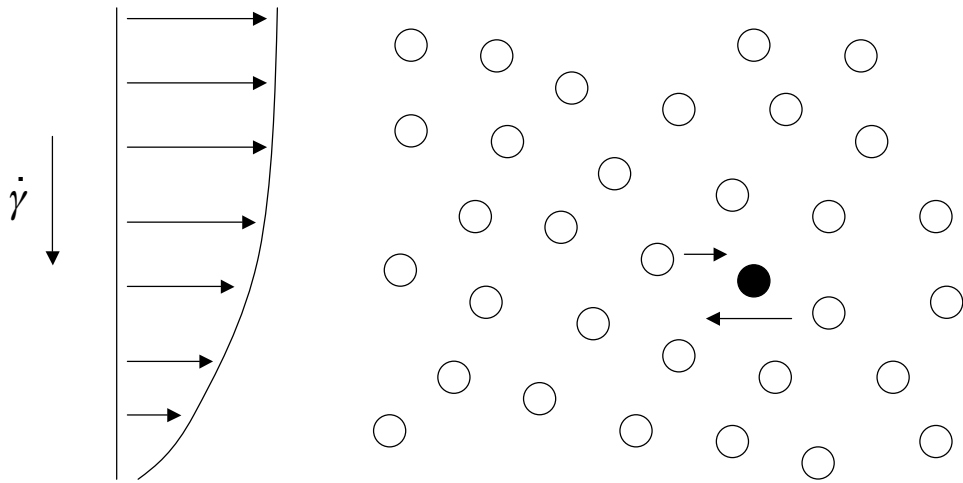
Figure 1.5: Influence of a non-uniform shear rate on migration. Since particle encounters occur at a rate proportional to the local shear, the suspension experiences a net particle flux toward low-shear regions.

contrast to purely hydrodynamic interactions between particles merely passing near each other, which are governed by the time-reversible Stokes equations and therefore cannot describe a diffusive process. The first effect is that in a concentration gradient, a test particle will interact with more neighbors on the high-ϕ side, which will tend to move it opposite the gradient (figure 1.3). This leads to a flux proportional to $\dot{\gamma}a^2\phi\nabla\phi$ when $\nabla\phi$ is perpendicular to the velocity. A second effect arises from concentration gradients because of the corresponding viscosity gradient. When two particles come into contact in a concentration gradient, the low-μ end of the two-particle body will be more free to move than the high-μ end, resulting in a net displacement in the direction of decreasing ϕ (figure 1.4). The flux from this effect is then expected to be proportional to $(\dot{\gamma}a^2\phi^2/\mu)(d\mu/d\phi)\nabla\phi$. The third effect is that when there is a gradient in the scalar shear rate, there will again be an excess of interactions on the high-shear side of a test particle, tending to move the particle toward low-shear regions (figure 1.5). Gradients in shear stress σ can then be expected to produce a particle flux proportional to $\dot{\gamma}a^2\phi^2/\sigma\nabla\sigma$. All three effects are justified only when the relevant gradients are normal to the velocity.

This model of shear-induced migration was used to successfully analyze a number of flows, including the viscous resuspension of particles from a settled bed [LA86], which had previously been assumed to require turbulence. However, the model as formulated by Leighton and Acrivos only describes flows in which the gradients in concentration and shear stress are either parallel or normal, and both are normal to the velocity. The model was extended to more general flows by Phillips et al. [PAB92] in 1991. In this form, the effects are divided into those due to anisotropic collision frequencies, with a coefficient K_c, and anisotropic response to collisions, with a coefficient K_μ. They then express the total flux in

an Eulerian frame in conservation form

$$\frac{D\phi}{Dt} = a^2 K_c \nabla \cdot (\phi^2 \nabla \dot{\gamma} + \phi \dot{\gamma} \nabla \phi) + a^2 K_\mu \nabla \cdot \left(\dot{\gamma} \phi^2 \frac{1}{\mu} \frac{d\mu}{d\phi} \nabla \phi \right), \qquad (1.25)$$

where $D/Dt = \partial/\partial t + v \cdot \nabla$ is the material derivative. While this model is still derived from the causes described by Leighton and Acrivos, which are restricted to gradients normal to the velocity, the Phillips et al. model is the simplest possible generalization to arbitrary flows. Phillips et al. were able to compare their model to experiments in a nonhomogeneous wide-gap Couette flow aided by NMR imaging, which allows the measurement of the concentration without disturbing the flow. This allowed the parameters to be measured as well, and they found the best fit for $K_c = 0.41$ and $K_\mu = 0.62$.

A separate 'suspension balance' model was introduced by Nott and Brady [NB94] in 1994 motivated by an analogy with the kinetic theory of gasses. They defined several macroscopic quantities in terms of particle properties without reference to the suspending fluid, including an average velocity, a stress tensor, and a 'temperature' representing velocity fluctuations about the mean. This model was found to offer better predictions in Poiseuille flow than the previous 'diffusive flux' models. In Poiseuille flow, a Newtonian fluid adopts a parabolic profile, with a maximum at the centerline and zero velocity at the walls, and both models predict a higher concentration at the center where the shear is lower. The diffusive flux models, however, predict that since by symmetry the shear rate must vanish at the center, ϕ must reach ϕ_m regardless of the average concentration, which results in a sharp cusp in the concentration profile. While the suspension balance model allows fluctuational motion to originate only from shear stress, this random motion is also allowed to diffuse analagous to heat in a gas, resulting in a positive temperature at the center and therefore smooth concentration profiles. Nott and Brady discuss finite particle size effects as a

mechanism for such heat transfer. They find the suspension balance model agrees well with numerical simulations, and generalizes more naturally to fully three-dimensional inhomogeneous flows. Drawbacks to this model include increased complexity and the need for more modeling functions to be determined, such as the viscosity and heat flux of the particle phase.

A further conceptual difference between the two models is that Nott and Brady describe the particle pressure as the fundamental result of particle interactions. They then determine the resulting particle fluxes which correspond to Leighton and Acrivos's shear-induced migration via the hindered settling function in the same manner as a gravitational stress. Brady and Morris [MB98] later generalized the suspension balance model to include anisotropic interactions, which are characterized by three normal stresses rather than a single pressure.

Nott and Brady also note that although the Stokes equations are in theory reversible, there is a finite 'domain of reversibility' in time after which this reversibility is not realistic. This is because even though the Stokes equations governing the fluid for known particle positions are linear in the particle velocities, they are nonlinear in the particle positions and result chaotic motion. Small perturbations introduced by thermal fluctuations, for example, or truncation and roundoff error in numerical simulations, will therefore be eventually amplified, destroying the time-reversible symmetry in real systems. For this reason, Nott and Brady argue that there is no contradiction in attributing shear-induced diffusion to hydrodynamic interactions, and the contact forces discussed by Leighton and Acrivos are unnecessary.

1.2.4 Numerical Simulations

The most popular method of simulating viscous suspensions is known as 'Stokesian dynamics', and was devised by Brady and Bossis in 1988 [BB88]. The method is modeled after molecular dynamics, in which large ensembles of atoms or molecules are evolved by calculating pairwise forces of interaction. This technique is possible in Stokes flow because, given the positions of particles, the specification of hydrodynamic forces and torques e.g. by gravity and no inertia act as boundary conditions on the particle surfaces that uniquely determine the fluid velocity and pressure everywhere. These fluid properties then are sufficient to determine the translational and angular velocities of all particles. Both of these calculations are linear and invertible, and can therefore be consolidated as a single linear system from which the particle evolution is determined, having eliminated all reference to the suspending fluid.

Simulation results [FB00, SB02] are generally in agreement with experiments for the mixture viscosity, although above approximately 50% concentration experimental measurements begin to vary, due to non-Newtonian behavior and clustering. Similarly, migration effects, also known as normal stress differences, are in agreement between simulation and experiment. Simulations of sedimenting mixtures tend to show the same divergent velocity fluctuations predicted in theory, which is at odds with most experiments. Early Stokesian Dynamics simulations were restricted to 50-200 particles arranged in a 'periodic monolayer' [CP94, BLS95], due to computational limitations, however increased processing power and a faster algorithm [SB01] now allow fully three-dimensional simulations involving at least 1000 particles.

1.2.5 Other Complex Fluids

Some similarities can be found in the dynamics of dry granular flows. Since air is still present in almost all granular flows, they are distinguished from suspensions primarily by the dominance of particle inertia over fluid viscosity, which is measured by the Bagnold number [Bag54]. Granular flows are extremely complex, as the materials can change from a plastic solid to a viscous liquid to an inelastic gas as the velocity increases. Determining an appropriate constitutive relation for granular materials remains a significant modeling challenge.

The work of Pouliquen et al. on granular chute flows is particularly relevant to this discussion because the geometry is similar to a gravity-driven thin film. Surface roughness is crucial for such experiments: with smooth surfaces a flow will either come to a stop at small inclination angles θ or accelerate indefinitely at larger θ, with a steady flow occurring only at a critical value of θ. Such flows are well described by a constant friction coefficient. On rough surfaces there is a finite range of θ for which stationary flows are reached, which suggest a more liquid-like model. A fingering instability arises in these flows with much the same shape as in liquid films, however the mechanism is different, involving vertical segregation of the particles based on size [PDS97]. With monodisperse particles the front does not finger.

Pouliquen found [Pou99] that the smallest angle θ_{stop} for which steady flow is possible decreases monotonically with the thickness h of the material, so the same information is contained in the function $h_{stop}(\theta)$. He used this fact to rescale his measurements of the average velocity, and found that the dimensionless velocity $u/\sqrt{gh}$ is linearly proportional to the ratio $h/h_{stop}(\theta)$, with the proportionality constant independent of θ. One model for the constitutive relation for this type of flow was proposed in 2006 by Jop et al. [JFP06], and is characterized by a yield

stress criterion and an effective viscosity that is proportional to the pressure and inversely proportional to the shear rate. The latter fact invites comparison to the suspension balance model of Nott and Brady, where the particle contributions to the pressure and viscosity are proportional.

Another related problem is the evolution of thin films in the presence of surfactant, which occurs in human lungs both naturally and as a method of drug delivery. One of the earliest mathematical treatments of this system is that of Jensen and Grotberg in 1992 [JG92]. Assuming weak capillarity and surface diffusion, they analyzed the rate of spreading caused by Marangoni forces. They derived spreading rates in terms of the rate surfactant is added to the system, and found that a shock exists at the leading edge of the surfactant. For slow influxes, the diffusive shock width ultimately increases faster than the spreading rate, eventually destroying the shock and leading to diffusive spreading. They also describe a thinning that occurs behind the shock that in experiments has led to film rupture, and propose a model for rupture based on van der Waals forces.

Other studies have focused on an instability observed in experiments, in which long dendritic fingers emanate from a drop of surfactant placed on an uncontaminated film. Warner, Craster, and Matar [WCM04] found a likely mechanism for this instability, involving a nonlinear equation of state by which the surface tension is determined from the surfactant concentration. They found a time-dependent base state for a symmetrical problem and performed a linear stability analysis, which revealed an instability consistent with the experimental literature. A subsequent analysis by Levy and Shearer [LS06] with both gravity and Marangoni driving forces found comparable solutions, and characterized the underlying shock and rarefaction dynamics. They found that while the system is not hyperbolic but mixed hyperbolic-parabolic, the techniques of hyperbolic systems

are useful to describe the essential features of the solutions.

1.3 Particle-laden Films

Only a few studies have been done that specifically explore particle laden thin films. One theoretical study by Schaflinger, Acrivos, and Zhang [SAZ90] applies the diffusive flux suspension model to two flow geometries, a film and a Poiseuille flow. They analyzed a film on an incline at steady state, by assuming no variation in the flow-wise and span-wise directions. In the depth-wise direction they obtained a condition for stationary flows by balancing gravitational settling with shear-induced diffusion. For simplicity they considered only diffusive fluxes, i.e. resulting from the gradient in concentration and not from the gradient in shear rate. Consequently in their equilibrium profiles the concentration is greatest at the bottom and decreases with height. As a boundary condition they matched the liquid and particle fluxes of the steady state profile to a well-mixed inflow. Since the particles in the steady solutions are concentrated more in the slower moving bottom of the film, matching fluxes results in a greater average concentration in the steady film than the inflow. For sufficiently concentrated inflow they found there is no steady solution, and particles simply pile up near the inlet.

Li and Pozrikidis [XP03] conduced a numerical simulation of a neutrally buoyant suspension in two dimensional film flow. The Stokesian dynamics numerical method is not easily extended to flows with a free surface; they used a boundary element method to solve for the Stokes flow outside of circular and elliptical particles in the plane, and their method also allowed the free surface of the fluid to deform due to the presence of the particles. While this method is easy to extend to arbitrarily shaped particles and emulsions of drops, the computational efficiency suffers at moderately high concentrations. Their simulation at 10% con-

centration found particles tending away from both the solid boundary and free surface toward the center of the film, however computational speed prevented the use of enough particles for statistical results.

More recently an experimental study was performed by Timberlake and Morris [TM05] of inclined film flow containing neutrally buoyant particles. In their experiments a gate was used upstream to maintain a steady influx of mixture, and downstream from the gate the film depth was found to decrease slowly in the direction of flow x. They were able to measure the suspension velocity using a stereoscopic photographic technique and particle correlation velocimetry. Although they were not able to directly measure the vertical positions of particles, they inferred from their velocity data that the concentration was somewhat greater near the free surface and vanished near the bottom. This is consistent with theories of migration, since the shear stress and shear rate both vanish at the free surface.

Timberlake and Morris also applied the suspension balance model of Nott and Brady [NB94] to this problem, enforcing constant flux of material independent of x. Unlike Acrivos et al., they imposed a finite normal stress jump at the free surface, representing their experimental observation that the surface becomes rough on the scale of the particle size. They found reasonable agreement between the model and experiment for the film depth and concentration profile, but the model failed to predict zero concentration near the solid boundary as seen in the experiment.

Another recent experiment was performed by Zhou, Dupuy, Bertozzi, and Hosoi [ZDB05, Zho04], using heavy particles. They used the same constant flux flow geometry as Timberlake and Morris, and found that rather than reaching a steady state the film displays one of three settling behaviors as it advances.

At low inclination angles and concentrations, the particles settle out of the flow leaving a film of clear fluid, while at intermediate angles and concentrations the suspension appeared well-mixed for the duration of the experiment. At high angles and concentrations the particles accumulate near the moving contact line in a "particle-rich ridge". They performed enough experiments with varied angles and concentrations to construct a phase diagram for the three settling behaviors. They also observed that while the fingering instability typical of pure liquid films occurs in the first two regimes, it is largely suppressed when the ridge appears.

Zhou et al. also introduced a model to describe this third regime, characterized by spatially varying rheology, which appears to have no analogue in pure fluid motion. They did not include shear induced diffusion, and attributed the particle accumulation at the contact line to gravitational settling in the flow direction. The main ingredients then were a hindered settling function to determine the relative velocities of the two phases, and an effective viscosity which controls the average velocity. In order apply lubrication theory they also found it necessary to assume the concentration is independent of the depth coordinate z, an assumption that will be discussed below. They were then able to derive a system of two coupled fourth-order evolution equations similar to the single fluid lubrication equation. They also argued that the large scale evolution of that system is determined by the 'reduced' system obtained by retaining only first-order derivative terms, much like the first-order equation 1.6 studied by Huppert captures many of the features of equation 1.19.

These reduced equations, which take the form of a 2×2 system of conservation laws, were briefly studied in Zhou et al.'s work. They found double-shock solutions for this system depending on the precursor thickness b used in the boundary condition, and the region between the shocks was thicker and higher in concen-

tration much like the observed ridge. They also noted that the speeds of the two shocks become nearly equal at small values of b, though their calculations were not sufficient to determine whether equality is attained at finite b or in the limit $b \to \infty$ or not at all. This issue is significant because if the speeds actually coincide at some $b^* > 0$ the existence of shock solutions for $b < b^*$ would be called into question. Furthermore, they described the physical derivation and the shock solutions only briefly, and a more complete description of the solutions is needed in order to understand the consequences of this model.

CHAPTER 2

Derivation of a Lubrication Model

In this chapter a lubrication model for particle-laden thin films will be derived following the techniques of Zhou [Zho04] and Zhou et al. [ZDB05], in order to describe the particle-rich ridge regime. Since depth-averaging of the equations of motion is an essential feature of lubrication models, an assumption will be needed about the vertical stratification of the flow. This assumption, that the particle concentration is independent of z, will be discussed further below, and a second model will also be derived in chapter 5 which allows for stratified films.

Since shear-induced migration will not be included in the basic model, it is not necessary to choose between the suspension balance and diffusive flux techniques. Still there is a basic choice to be made in the dependent variables. "Two-fluid" models specify the velocities of each phase, which are coupled by drag forces, while "one-fluid" models specify instead average and relative velocities [Ung93]. Following Zhou et al. [ZDB05] this work will use a one-fluid model, which is generally more convenient for viscous suspensions because strong drag forces typically ensure that the relative velocity is small.

Deriving a one-fluid model involves balancing forces first for the mixture as a whole, without regard to interactions between the two components. In the present case inertia is negligible, and these forces are just gravity and viscous stress. We use an empirical expression for the latter in which the mixture is considered a Newtonian fluid, with an effective viscosity depending on the particle volume

fraction ϕ. For a fluid of kinematic viscosity μ_f one form for this relation is [Kri72, SP05]

$$\mu(\phi) = \mu_f(1 - \phi/\phi_m)^{-2}, \tag{2.1}$$

where $\phi_m \approx 0.67$ is the random packing fraction of spheres. This viscosity leads to a stress tensor of the form

$$\mathbf{\Pi} = p\mathbf{I} - \frac{1}{2}\mu(\phi)\left[\nabla\mathbf{v} + (\nabla\mathbf{v})^T\right], \tag{2.2}$$

where p is the fluid pressure and $\mathbf{v}$ is a velocity characterizing the motion of the mixture. Since the two mixture components in general have different velocities, say v_f and v_p for the fluid and particulate phases respectively, $\mathbf{v}$ must be some average of the two. Much of the experimental literature deals with neutrally buoyant mixtures, in which the two velocities are the same and the distinction is unnecessary, but in the current case the question is relevant. We argue that since the effective viscosity phenomenon involves neither inertia nor gravity, it should be independent of the masses of the two phases, therefore we select the volume-averaged velocity. The one-fluid variables are thus

$$\mathbf{v} = (1 - \phi)\mathbf{v_f} + \phi\mathbf{v_p}, \qquad \mathbf{v_{rel}} = \mathbf{v_p} - \mathbf{v_f}, \tag{2.3}$$

and the individual phase velocities can be recovered by

$$\mathbf{v_p} = \mathbf{v} + (1 - \phi)\mathbf{v_{rel}}, \qquad \mathbf{v_f} = \mathbf{v} - \phi\mathbf{v_{rel}}. \tag{2.4}$$

The average velocity satisfies the Stokes equations:

$$\nabla \cdot \mathbf{\Pi} = \rho(\phi)\mathbf{g}, \qquad \nabla \cdot \mathbf{v} = 0, \tag{2.5}$$

where $\rho(\phi)$ is the mixture density and $\mathbf{g}$ is the gravitational field. The density is given by $\rho(\phi) = \rho_f(1 + \Delta\phi)$, where $\Delta = (\rho_p - \rho_f)/\rho_f$ and ρ_f and ρ_p are the densities of the fluid and particulate phases.
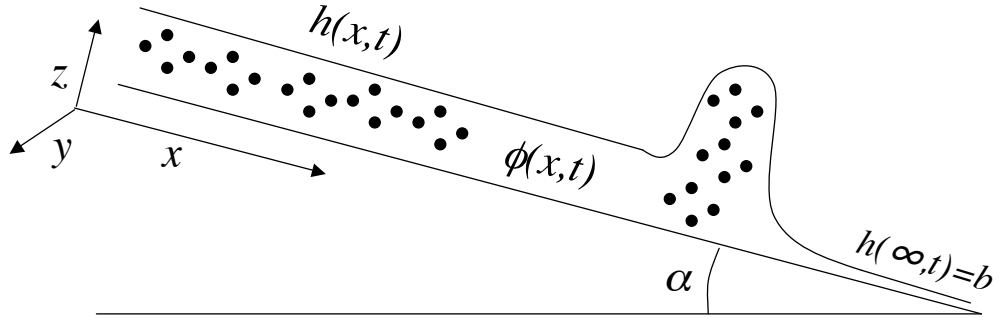
Figure 2.1: Geometry of the particle-laden film. b represents the precursor, discussed below.

We now define the problem geometry as in figure 2.1, considering a plane solid surface inclined at an angle θ to the horizontal, to be coated with an advancing gravity-driven film. We choose a coordinate system in which $\mathbf{z}$ is normal to the inclined plane, $\mathbf{x}$ and $\mathbf{y}$ lie in the inclined plane, $\mathbf{y} \cdot \mathbf{g} = 0$, and suppose the film emerges from a gate at $x = 0$ at a constant thickness and particle concentration for $t > 0$.

In deriving the equation for $\mathbf{v}$, we follow the standard methods used for pure fluid films [Gre78, ODB97]. The lubrication approximation, valid at small Reynolds numbers and geometric aspect ratios, assumes $\mathbf{v}$ lies in the $\mathbf{x}$-$\mathbf{y}$ plane and $\left| \frac{\partial \mathbf{v}}{\partial z} \right| \gg \max \left(\left| \frac{\partial \mathbf{v}}{\partial x} \right|, \left| \frac{\partial \mathbf{v}}{\partial y} \right| \right)$. Correspondingly, we now consider all velocities to be two-dimensional vectors, as well as the gradient $\nabla = \mathbf{x} \frac{\partial}{\partial x} + \mathbf{y} \frac{\partial}{\partial y}$, and define $g_\perp = \mathbf{g} \cdot \mathbf{z} = |\mathbf{g}| \cos \theta$ and $\mathbf{g}_\parallel = \mathbf{g} - g_\perp \mathbf{z} = (|\mathbf{g}| \sin \theta) \mathbf{x}$. In this notation, the Stokes

equations now read

$$\frac{\partial p}{\partial z} = -\rho(\phi)g_\perp, \tag{2.6a}$$

$$\nabla p = \mu(\phi)\frac{\partial^2 \mathbf{v}}{\partial z^2} + \rho(\phi)\mathbf{g}_\parallel. \tag{2.6b}$$

The Laplace-Young boundary condition states that the pressure at the free surface, $z = h(x, y)$, is given by

$$p(x, y, h(x, y)) = -\gamma\nabla^2 h(x, y) \tag{2.7}$$

where γ is the coefficient of surface tension. The pressure is then determined by

$$p(x, y, z) = -\gamma\nabla^2 h(x, y) + \int_z^{h(x,y)} \rho(\phi(x, y, z'))g_\perp dz' \tag{2.8}$$

from the depth and particle concentration of the film. Here it is convenient to assume the particle concentration is independent of the z coordinate, so that the integral in (2.8) is merely $\rho(\phi)g_\perp(h - z)$. We will discuss this assumption further in our treatment below of particle motion.

Combining (2.6b) and (2.8) and defining $P(x, y) = -\gamma\nabla^2 h + \rho(\phi)g_\perp h$, we have

$$\nabla P - zg_\perp\nabla\rho = \rho(\phi)\mu(\phi)\frac{\partial^2 \mathbf{v}}{\partial z^2} + \rho(\phi)\mathbf{g}_\parallel. \tag{2.9}$$

The boundary conditions of interest are no stress ($\partial\mathbf{v}/\partial z = 0$) at the free interface and no slip ($\mathbf{v} = 0$) at the solid interface. Equation (2.9) can now be integrated twice in z with the constants of integration determined by these conditions, to arrive at the equation

$$\mu(\phi)\mathbf{v} = (hz - \frac{z^2}{2})(\rho(\phi)\mathbf{g}_\parallel - \nabla P) + \frac{1}{2}(h^2 z - z^3/3)g_\perp\nabla\rho(\phi) \tag{2.10}$$

for the volume-averaged velocity. Integrating once more gives the depth-averaged velocity

$$\mathbf{v_{av}} = \frac{h^2}{3\mu(\phi)}\left[\gamma\nabla\nabla^2 h - g_\perp\left(\nabla(\rho(\phi)h) - \frac{5}{8}h\nabla\rho(\phi)\right) + \rho(\phi)\mathbf{g}_\parallel\right]. \tag{2.11}$$

41

Modeling the relative velocity due to particle settling turns out to be more difficult. Recall that in the above lubrication analysis, we have assumed the particles are evenly distributed across the film depth. Realistically this assumption is not justified and is used here only for simplicity. The vertical distribution of particles involves a balance between gravitational settling and shear-induced migration, and is studied in chapter 5.

Nevertheless we use the uniform vertical distribution $\phi = \phi(x, y, t)$ on the following grounds. Zhou et al. found that particles settle out of the fluid only at low angles and concentrations, so some depth profile must exist. An experiment and theory by Timberlake and Morris with neutrally buoyant particles found $d\phi/dz > 0$ [TM05], due to shear-induced particle migration [LA87]. However Schaflinger et al. [SAZ90] considered heavy particles in their analysis and found $d\phi/dz < 0$. Also the analysis in chapter 5 demonstrates that both increasing and decreasing depth profiles are possible, depending on ϕ and α. Since it is unclear even whether the actual concentration profile for film flow increases or decreases with depth, and since we are seeking a simple model, the uniform depth profile appears reasonable.

We begin our model of the expression (1.22) for the settling velocity, and using the Richardson-Zaki hindered settling function

$$\mathbf{v} = f_{RZ}(\phi)\mathbf{v_s} = (1 - \phi)^n \mathbf{v_s} \tag{2.12}$$

where $n \approx 5$ for Stokes flow [RZ54]. We also seek a correction to represent the impeding effect of the solid substrate on particle motion. The Stokes problem for a sphere settling in a half-space parallel to a wall has been solved approximately by the method of images [HB65], leading to the series solution

$$\mathbf{v} = \left(1 - \frac{259}{256}\left(\frac{a}{h}\right) + \frac{9}{16}\left(\frac{a}{h}\right)\log\left(\frac{a}{h}\right) - \frac{1}{16}\left(\frac{a}{h}\right)^3 + \frac{15}{256}\left(\frac{a}{h}\right)^4 + ...\right)\mathbf{v_s} \tag{2.13}$$

for the velocity, where $h > a$ is the distance from the center of the particle to the wall. Since we seek a depth-averaged solution we are concerned not with the velocity itself, but its average value over the interval $(0, h)$. Figure 2.2 shows this average for a range of h/a, where the velocity has been taken to be zero for $h < a$. Also plotted is the correction we will use to approximate wall effects:

$$w(h) = \frac{A(h/a)^2}{\sqrt{1 + \left[A(h/a)^2\right]^2}} \tag{2.14}$$

with $A = 1/18$. This function has the desired properties $w \approx 0$ for $h < a$, $w \approx 1$ for $h \gg a$, and unlike equation (2.13) is differentiable and positive on $(0, \infty)$. We have chosen the parameter A so that this function resembles (2.13), but since the latter neglects the net flow and the effects of other particles it should mainly be viewed as a correction to ensure $\mathbf{v_{rel}} \to 0$ for very thin films.

For lack of a comprehensive theory incorporating both wall effects and hindered settling, we simply assume the effects are multiplicative, obtaining the settling velocity

$$\mathbf{v_{rel}} = f(\phi)w(h)\mathbf{v_s} \tag{2.15}$$

relative to the fluid which we interpret as a depth average. Having specified the two velocities required for a one-fluid description, we apply conservation of volume to the mixture as a whole and separately to the particulate phase, obtaining the evolution equations[1]:

$$\frac{\partial h}{\partial t} + \nabla \cdot (h\mathbf{v_{av}}) = 0,$$
$$\frac{\partial \phi h}{\partial t} + \nabla \cdot (\phi h\mathbf{v_p}) = 0. \tag{2.16}$$

Inserting equations (2.11), (2.15), and (2.4) into (2.16) now gives us the complete system

---

[1]In [ZDB05] both terms of the first equation of (2.16) had an extra factor of $\rho(\phi)$, due to the use of a mass-averaged rather than volume-averaged velocity in constructing the stress tensor. This error appears to leave the qualitative properties of the model unchanged.
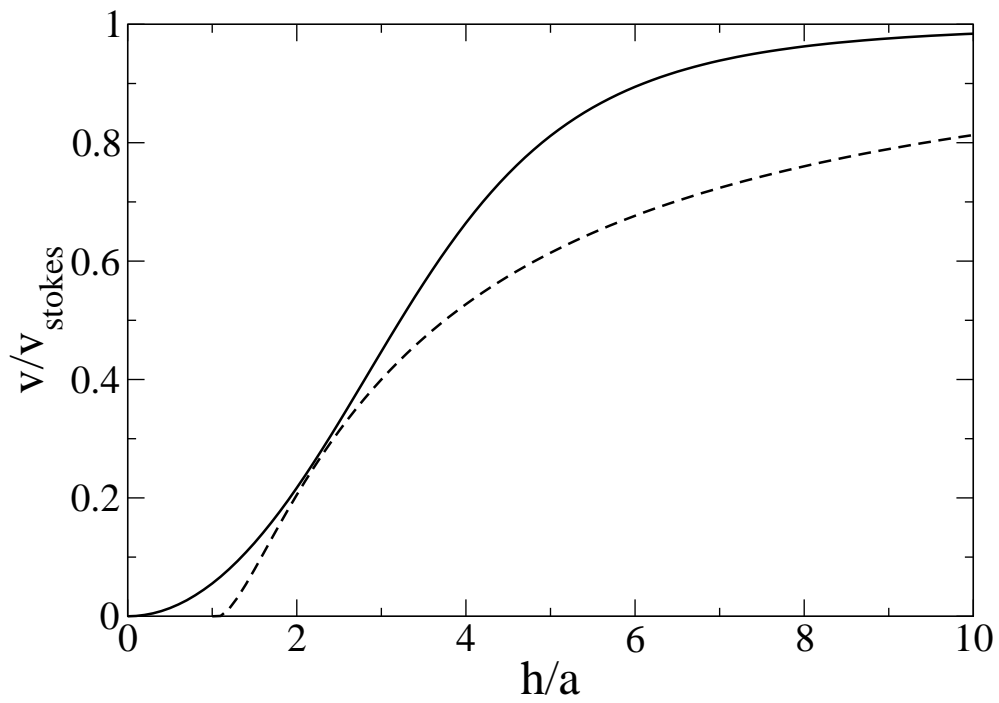
Figure 2.2: Our correction for the impeding effect of the solid boundary on a single particle's settling velocity (solid), and an analytical result neglecting the free surface and large-scale fluid motion (dashed).

$$\frac{\partial h}{\partial t} + \nabla \cdot \left(\frac{h^3}{3\mu(\phi)} \left[\gamma \nabla \nabla^2 h - g_\perp \left(\nabla(\rho(\phi)h) - \frac{5}{8} h \nabla \rho(\phi) \right) + \rho(\phi) \mathbf{g}_\parallel \right] \right) = 0,$$

(2.17a)

$$\frac{\partial (\phi h)}{\partial t} + \nabla \cdot \left(\frac{\phi h^3}{3\mu(\phi)} \left[\gamma \nabla \nabla^2 h - g_\perp \left(\nabla(\rho(\phi)h) - \frac{5}{8} h \nabla \rho(\phi) \right) + \rho(\phi) \mathbf{g}_\parallel \right. \right.$$
$$\left. \left. + \phi h(1 - \phi) f(\phi) w(h) \mathbf{v_s} \right) = 0. \right.$$

(2.17b)

Next we nondimensionalize the equations for the constant flow rate problem, with the rescaling used in [BB97] for a clear fluid. If the upstream gate height h_0 represents a typical film thickness, then the first- and fourth-order terms in (2.17) are comparable at a length scale $x_0 = (\ell^2 h_0)^{1/3}$, where $\ell = \gamma/\rho_f g_\parallel$ is the capillary length. The time derivative is on the same scale as well if $t \sim t_0 = \mu_f x_0/Ca\gamma$, where $Ca = h_0^2/3\ell^2$ is the dimensionless capillary number. Defining $\tilde{h} = h/h_0$, $\tilde{x} = x/x_0$, $\tilde{t} = t/t_0$, $\tilde{\rho}(\phi) = 1 + \Delta\phi$, $\tilde{\mu}(\phi) = (1 - \phi/\phi_{max})^{-2}$, $\tilde{w}(\tilde{h}) = w(h)$, and dropping the tildes, and replacing ∇ with $\partial/\partial x$ in anticipation of a y-independent solution, we obtain the dimensionless system

$$\frac{\partial h}{\partial t} + \frac{\partial}{\partial x} \left(\frac{h^3}{\mu(\phi)} \left[h_{xxx} - D(\theta) \left((\rho(\phi)h)_x - \frac{5}{8} h \rho(\phi)_x \right) + \rho(\phi) \right] \right) = 0$$

(2.18a)

$$\frac{\partial (\phi h)}{\partial t} + \frac{\partial}{\partial x} \left(\frac{\phi h^3}{\mu(\phi)} \left[h_{xxx} - D(\theta) \left((\rho(\phi)h)_x - \frac{5}{8} h \rho(\phi)_x \right) + \rho(\phi) \right] + \right.$$
$$v_s \phi h(1 - \phi) f(\phi) w(h)) = 0.$$

(2.18b)

Here $D(\theta) = (3Ca)^{1/3} \cot\theta$ is a parameter measuring the relative importance of the 2nd-order terms.

The above nondimensionalization represents the scales at which all terms in (2.17) are equally significant. However, at length scales $x \gg x_0$, the second- and

fourth-order terms become small, and can be considered simply a weak diffusive regularization to the dominant first-order system,

$$\frac{\partial h}{\partial t} + \frac{\partial}{\partial x}\left(h^3\rho(\phi)/\mu(\phi)\right) = 0 \qquad (2.19a)$$

$$\frac{\partial(\phi h)}{\partial t} + \frac{\partial}{\partial x}\left(\phi h^3\rho(\phi)/\mu(\phi) + v_s\phi h(1-\phi)f(\phi)w(h)\right) = 0. \qquad (2.19b)$$

Zhou et al. presented this alternative scaling and presented numerical evidence that the higher-order terms can be neglected. Note also that the second-order terms can also be dropped regardless of the length scale if $\theta = \pi/2$.

Following Zhou et al., we adopt the precursor model for the contact line because it simplifies the analysis by preserving the symmetry of the Riemann problem, discussed in chapter 3 below. With a precursor of nondimensional thickness $b \ll 1$ and concentration ϕ_R, the initial conditions for the constant flow rate problem are

$$(h,\phi)|_{t=0} = \begin{cases} (1,\phi_L) & \text{if } x < 0 \\ (b,\phi_R) & \text{if } x > 0 \end{cases}. \qquad (2.20)$$

Both b and ϕ_R are model parameters not determined by the bulk flow, and must be specified. Since the film depths are on the order of millimeters, meaningful values for b are between 10^{-6} and 10^{-1}, corresponding to precursors no thinner than the molecular scale. Reasonable values for the concentration ϕ_R are between 0 and ϕ_L. We mainly consider $\phi_R = \phi_L$ for definiteness, but also discuss $\phi_R = 0$.

The system (2.19) is related to thin film equations that have been studied for pure fluids, some of which were discussed in the introduction. If $\phi(x,t) \equiv 0$ or more generally $\phi \equiv \phi_0 \geq 0$ and $a \to 0$ (so that $\mathbf{v_s} = 0$), the system degenerates to the single equation (1.6) studied by Huppert [Hup82] which has single shock solutions to the Riemann problem. Bertozzi et al. studied a variant of (1.6) in which Marangoni forcing competes with gravity, resulting in more complex

shock structures [BMS99]. Lubrication models have given rise to pairs of coupled equations describing a thin films containing surfactant [IM98, LS06]. Also related are models for sedimenting mixtures [Kyn52] in which the particle concentration exhibits kinematic shocks.

CHAPTER 3

Hyperbolic Theory and the Reduced Equations

3.1 Conservation Laws

Before analyzing the reduced system (2.19), it is necessary to review the theory of systems of nonlinear conservation laws in one dimension. Conservation laws are equations of the form

$$\frac{\partial U}{\partial t} + \frac{\partial}{\partial x} F(U) = 0, \qquad U, F(U) \in \Omega \subset \mathbb{R}^n. \tag{3.1}$$

Although initial-value problems for (3.1) are not in general well-posed, there is a large body of analytical techniques for finding and characterizing solutions when they exist [Lax73]. The analysis is especially simplified for the Riemann problem, in which the initial data is a step function

$$U(x,0) = \begin{cases} U_L & \text{if} \quad x < 0 \\ U_R & \text{if} \quad x > 0 \end{cases}, \tag{3.2}$$

such as (2.20) with uniform concentration.

Both the equation and initial data of the Riemann problem can be expressed in terms of the single variable $\xi = x/t$, and this symmetry extends to solutions as well. Imposing this form on the solution reduces the problem to finding a heteroclinic orbit for the autonomous system

$$\left[J\big(U(\xi)\big) - \xi I \right] \dot{U}(\xi) = 0, \tag{3.3a}$$

$$U(-\infty) = U_L, \qquad U(+\infty) = U_R, \tag{3.3b}$$

where $J(U)$ is the Jacobian derivative of the flux function F. Smooth solutions of (3.1), known as rarefactions, are therefore either constant or vary along integral curves R_i of a Jacobian eigenvector r_i. For this reason, most existence results apply to strictly hyperbolic systems, in which the eigenvalues are real and distinct.

Equation (3.3a) also requires that rarefaction solutions be parametrized by the corresponding eigenvalue λ_i, which is possible only if λ_i is strictly increasing on R_i between U_L and U_R. We discuss here the simplified case when F satisfies the genuine nonlinearity condition, that λ_i varies strictly monotonically along R_i for all i and R_i, and consider the more general case in the appendix.

In a genuinely nonlinear system $R_i(U)$ consists of two connected curves $R_i^+(U) = \{U' \in R_i(U) | \; \lambda_i(U') > \lambda_i(U)\}$ and $R_i^-(U) = \{U' \in R_i(U) | \; \lambda_i(U') < \lambda_i(U)\}$, and a connecting orbit exists when $U_L = U$ and $U_R \in R_i^+(U)$, or $U_R = U$ and $U_L \in R_i^-(U)$. Consequently smooth solutions do not exist for general data, and solutions are generally sought from the larger class of weak solutions.

A weak solution to the conservation law (3.1) is an L^∞ function $U(x,t)$ that in addition to the initial condition satisfies

$$\int_{x_1}^{x_2} \big(U(x,t_2) - U(x,t_1)\big)dx + \int_{t_1}^{t_2} \big(F(U(x_2,t)) - F(U(x_1,t))\big) = 0 \tag{3.4}$$

for all $x_2 > x_1$ and $t_2 > t_1 > 0$. This includes all smooth solutions to (3.1), but also allows discontinuities along a curve $x = st$ that satisfies the vector Rankine-Hugoniot condition

$$F(U^+) - F(U^-) = s\big(U^+ - U^-\big) \tag{3.5}$$

where U^- and U^+ are the values of U on either side of the discontinuity. The Hugoniot locus $H(U^-)$ is defined as the set of U^+ that satisfy (3.5) for some s. [Note that while the symmetry of (3.5) implies $U_2 \in H(U_1)$ is equivalent to

$U_1 \in H(U_2)$, it does not follow that $H(U_1) = H(U_2)$].

Such weak solutions are not unique, however, and a method must be chosen to select a single solution. Various criteria, known as entropy conditions, have been proposed in order to distinguish the shock, or admissible discontinuity, from any other weak solutions. One condition, the method of viscous profiles, is motivated by the fact that conservation laws often appear physically as approximations to higher-order regularized equations such as

$$\frac{\partial}{\partial t}U^\epsilon + \frac{\partial}{\partial x}F(U^\epsilon) = \epsilon\frac{\partial^2}{\partial x^2}U^\epsilon \tag{3.6}$$

which are well-posed for $\epsilon > 0$. A solution to (3.1), according to this method, should be stable in the sense that it appears as the pointwise limit in x, t of solutions U_ϵ to (3.6) as $\epsilon \to 0$. This condition has the advantage of a clearly desirable physical interpretation that assures shock solutions are unique, however it has the drawback of being difficult to verify.

A simpler method from the analytical perspective is the Lax entropy condition, which is equivalent to the viscous profile condition for a certain class of scalar conservation laws. This method relies on strict hyperbolicity to index the eigenvalues λ_i of $J(U)$ in increasing order for each U. These eigenvalues represent the characteristic speeds at which the equation propagates information, as can be seen in rarefaction solutions to the Riemann problem in the persistence of the left state U_L for $x \leq \lambda_i(U_L)t$ and the right state U_R for $x \geq \lambda_i(U_R)t$. The Lax entropy condition requires the discontinuity be continually reinforced by conflicting information from a single characteristic field, i.e. it moves with a speed s that satisfies

$$\lambda_i(U_L) > s > \lambda_i(U_R) \tag{3.7}$$

for exactly one i. That characteristic is emphasized by calling the discontinuity an i-shock.

In a neighborhood of any U the Hugoniot locus $H(U)$ consists of two smooth curves intersecting at U, and the four branches leaving U correspond to the four cases of 1- or 2-shocks with U as the right or left state. We denote the continuations of these branches by U_i^+ if U is the left state and U_i^- if U is the right state. The allowable connections $C_i^+(U_L) = R_i^+(U_L) \cup S_i^+(U_L)$ through the i-th characteristic also locally form a smooth curve for each i. The variation of an i-shock or i-rarefaction solution is confined to the interval $\{\xi : \min(\lambda_i(U_L), \lambda_i(U_R)) < \xi < \max(\lambda_i(U_L), \lambda_i(U_R))\}$, so compound connections can be generated by stringing together waves of different characteristics as long as ξ increases with i. In fact, $\{C_i^+\}_{i=1}^n$ locally generate a smooth coordinate system, so if U_R is sufficiently close to U_L the Riemann problem is well-posed.

Existence of solutions for large data depends on the topology of $H(U)$. A famous example of a system with no solutions for certain Riemann data is the Keyfitz-Kranzer equation (3.8) [KK90], in which $H(U)$ is compact. A bounded Hugoniot locus implies a bound on the strength of a shock, and consequently some large-data Riemann problems have no weak solutions. Section 3.3 describes a theory for such systems relating the regularized profiles to a Dirac mass, however this theory is far from complete.

A final complication to the selection of weak solutions is the nature of the regularization actually present in the physical system. The Lax and Oleinik conditions are intended to admit those shocks that appear as viscous limits under the simplest possible regularization. If the actual regularization is different, the viscous profiles could converge to a weak solution other than that selected by the entropy criteria. This possibility is indeed relevant to conservation laws describing thin films, which are generally regularized by nonlinear fourth-order capillary terms such as in (2.18). In fact, a scalar thin film equation with similar regu-

larization is known to select an entropy-violating double-shock solution, rather than the single-shock entropy solution [BMS99].

3.2   Particular Solutions

Returning to the reduced system (2.19), we note that the equations are physically meaningful for (h, ϕ) in the phase space $\Omega = \{(h, \phi) : 0 < h,\ 0 < \phi < \phi_{max}\}$, which can also be expressed in terms of the conserved quantities $u \equiv h$ and $v \equiv \phi h$ as $\{(u, v) \in \mathbb{R}^2 : 0 \leqslant v < \phi_{max} u\}$. While the above theory depends on the latter parameterization, the flux functions are most simply expressed in terms of h and ϕ, so we retain these variables for presenting our results.

The simple connections for a left state of $(h_L, \phi_L) = (1.0, 0.3)$ are shown in figure 3.1. The rarefaction curves have been integrated from (3.3a) by a Runge-Kutta method, and $H(U_L)$ has been calculated by eliminating s from (3.5) at each point and solving the resulting equations for u and v. For a given shock connection, the shock speed can be recovered by substituting u and v back into (3.5).

Since h was rescaled by the film thickness set at the upstream gate, we choose $(h, \phi) = (1.0, 0.3)$ as the left state. For a specified right state (b, ϕ_R), representing the precursor film, a solution to the Riemann problem can be determined by finding intersections between the two connection diagrams. In figure 3.2 we have plotted the possible shock-shock connections for four values of b with $\phi_R = \phi_L$. At $b = 0.1$ there is a solution with a 1-shock from the upstream state to an intermediate height and concentration slightly larger, and a 2-shock from this intermediate state to the precursor. As the precursor becomes thinner, the height and concentration of this intermediate state increase. For $b = 0.01$ the inter-
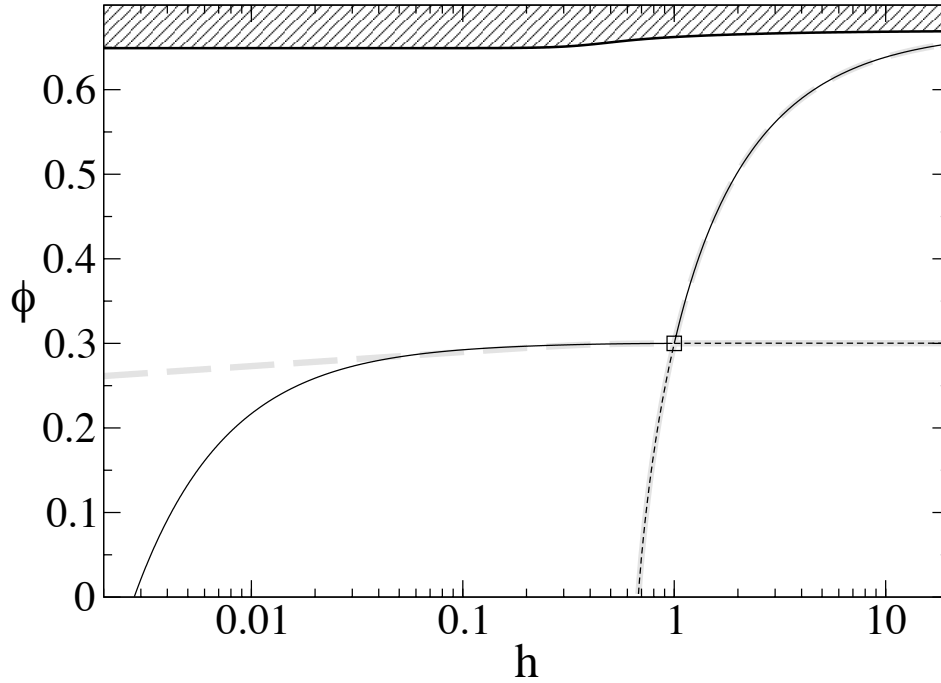
Figure 3.1: The phase space of the reduced model, and the connections from $(h_0, \phi_0) = (1.0, 0.3)$, $\square$. The system is hyperbolic except in the shaded region. Black lines represent shock connections and gray represents rarefactions. Solid lines are connections to the right, i.e. the (h_0, ϕ_0) is the left state, and dashed lines are connections to the left. 1-waves and 2-waves can be distinguished by their slope at (h_0, ϕ_0): 2-waves are nearly horizontal at this scale.

mediate state is approximately $(h, \phi) = (1.1757, 0.3663)$, and in figure 3.3 we compare this connection with a numerical solution with the same initial data, and find both shock speeds and the height and concentration of the ridge are in agreement. The numerical solution was calculated using the Lax-Freidrichs finite difference method with grid spacing 3.3×10^{-7} and timestep 3.3×10^{-7}.

At $b = 0.008$ the Hugoniot locus has undergone a bifurcation such that the 1- and 2-shock curves are no longer distinct, and an additional connected component has appeared. The shock speed and characteristic speeds coincide at several points along these curves, such that various sections correspond to 1-shocks, 2-shocks, or are not admissible at all. There is still a shock-shock connection that satisfies the Lax entropy condition. At $b = 0.0015$, however, there are no longer any intersections, and since the rarefactions also fail to intersect, this initial data has no solution. We will discuss this case further in §3.3.

As shown in figure 3.1, the equations using (2.12) are neither strictly hyperbolic nor genuinely nonlinear on this entire domain. Hyperbolicity fails near the maximum concentration, as the eigenvalues become complex and the equations become elliptic. It is not clear whether this feature is desired in a model of the thin film. Change of type certainly complicates the mathematical question of well-posedness for such a system, but remembering that the first-order system is only an approximation to the full fourth-order model, this is most likely an inconvenience rather than a physical flaw. Physical models proposed for dry granular materials result variously in hyperbolic, parabolic, and elliptic equations, so physically the change of type does not seem altogether unreasonable.

If the concentration in the precursor is taken to be 0 rather than ϕ_L, double-shock solutions again occur and the same non-existence issue occurs for small b. For larger b, an additional type of solution occurs consisting of a 1-rarefaction
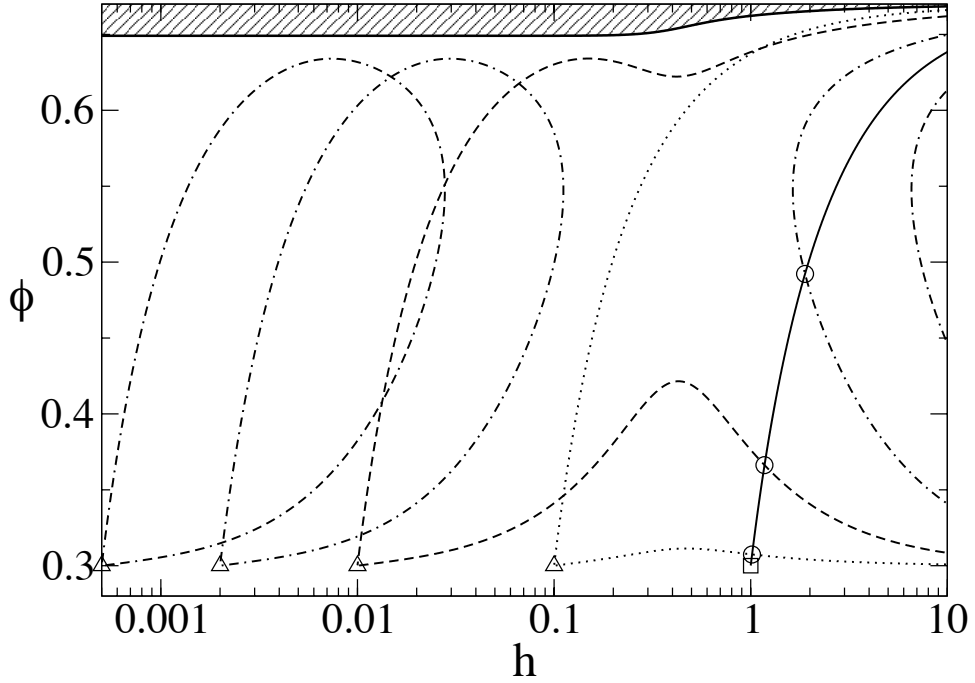
Figure 3.2: 1-shock connections (solid line) from an upstream state $(h_L, \phi_L) = (1.0, 0.3)$ ($\square$) and 1- and 2-shock connections from four precursor states $(h_R, \phi_R) = (b, 0.3)$ ($\triangle$) where $b = 0.1$ (dot), 0.01 (dash), 0.002 (dot-dash), and 0.0005 (dot-dash-dash). The solutions involve an intermediate state between the two shocks, marked by $\bigcirc$. As b becomes small, the Hugoniot locus undergoes a bifurcation, becoming disconnected, and ultimately fails to produce a shock solution.
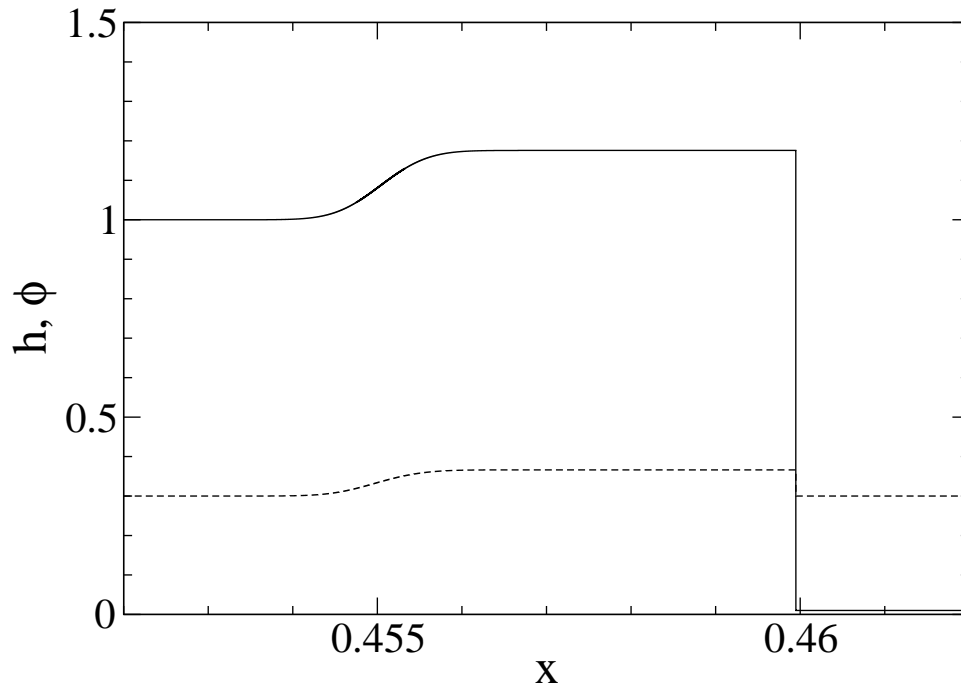
Figure 3.3: Film thickness (solid) and concentration (dashed) of a numerical solution of the conservation laws at $t = 1$, with $(h_L, \phi_L) = (1.0, 0.3)$ and $(h_R, \phi_R) = (0.01, 0.3)$. Numerical diffusivity generally affects the leading shock less than the trailing shock, since for the latter one of the characteristic speeds is close to the shock speed.

and a 2-shock, with both h and ϕ in the intermediate state less then their values at the left. A numerical solution for this case is shown in figure 3.4, again computed using the Lax-Freidrichs finite difference method in a moving frame. This behavior does not correspond to anything observed in the experiments of Zhou et al., and is probably observable only for heavily pre-wet substrates if at all.
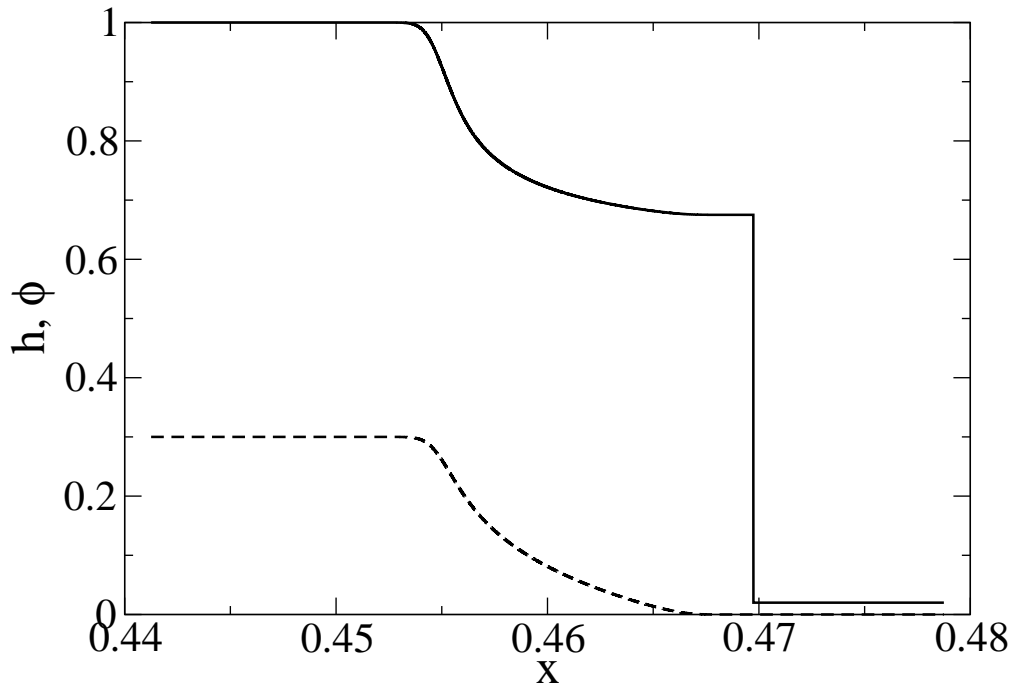
Figure 3.4: Numerical solution of the conservation laws at $t = 1$, with $(h_L, \phi_L) = (1.0, 0.3)$ and $(h_R, \phi_R) = (0.02, 0)$, corresponding to a 1-rarefaction and 2-shock. While some of the smoothness is due to numerical diffusivity, the 1-rarefaction can also be distinguished from a 1-shock by the fact that both h and ϕ are less than their values on the left.

3.3 Singular Shocks

The problem of non-existence due to non-trivial Hugoniot topology has been studied before, and a weaker form of solution known as a singular shock has been described. An illustrative example is the Keyfitz-Kranzer equation [KK90]

$$\frac{\partial}{\partial t}\begin{pmatrix} u \\ v \end{pmatrix} + \frac{\partial}{\partial x}\begin{pmatrix} u^2 - v \\ \frac{1}{3}u^3 - u \end{pmatrix} = 0, \tag{3.8}$$

which is everywhere both strictly hyperbolic and genuinely nonlinear, but for all $U = (u, v)$ the Hugoniot locus is compact, specifically figure-8 shaped. Thus shocks can only connect states that are sufficiently close, and certain Riemann problems have no classical solution.

In [KK95], Keyfitz and Kranzer present three sequences of functions $U^\epsilon(\xi = x/t)$ to (3.8) that approximately solve (3.8) as $\epsilon \to 0$ but are also singular in this limit. The first sequence results from an asymptotic expansion of the solution to the regularized equation

$$\frac{\partial U}{\partial t} + \frac{\partial}{\partial x}F(U) = \epsilon t\frac{\partial^2 U}{\partial x^2} \tag{3.9}$$

in ϵ, and the second and third are explicitly constructed from C^∞ functions and piecewise constant functions. They introduce a space of measures in which these sequences converge to a limit involving Dirac-like masses superimposed on a classical shock. They also propose overcompression as an admissibility requirement for singular shocks, i.e. (3.7) must hold for both characteristics; if singular shocks are accepted under this restriction (3.8) is well posed for all Riemann data. However, these conclusions are restricted to (3.8). Also, Keyfitz and Kranzer emphasize that while the limiting measures appear as limits of approximate solutions, no well-defined criterion has been proposed by which the limits themselves can be called solutions.

Sever discusses the selection mechanism for singular shocks in a more general context in [Sev07]. For a distribution solution

$$U(x,t) = M(t)\delta(x - st) + \begin{cases} U_L & \text{if } x < st \\ U_R & \text{if } x > st \end{cases} \tag{3.10}$$

characterized by a point mass $M(t)$ located at $x = st$, conservation implies the singular mass must satisfy

$$\frac{dM}{dt} = s(U_R - U_L) - \big[F(U_R) - F(U_L)\big]. \tag{3.11}$$

Since the speed s is unknown, this is an undetermined system for the $n + 1$ parameters dM/dt, s. For (3.8), Keyfitz and Kranzer determined unique solutions by requiring the first component of M to vanish, justified by an argument specific to that system. Sever writes that this last constraint generally comes from properties of the system such as symmetry groups or a convex entropy function. The proper constraint for system (2.19) is not yet apparent.

Equations (2.19) with regularization (3.6) also show behavior consistent with a singular shock. In order to investigate this, numerical solutions were generated with a fully implicit centered difference scheme on a moving nonuniform grid. The number of grid points at each mesh size was fixed, however every 10 time steps the grids were rearranged using cubic interpolation as necessary to center the area of maximum resolution around the singularity. Meanwhile the entire computational domain moved a constant speed chosen to approximately match the speed of the discontinuity. The scaling of the regularized solution satisfies $U^\epsilon(x,t) = U^1(\epsilon x, \epsilon t)$, so rather than take $\epsilon \to 0$ we fixed $\epsilon = 1$ and evaluated the solution at long times.

Figure 3.5 contains the results of this calculation. Both components of the singular mass increase linearly in time, as required by (3.11), and the singularity

is overcompressive. As the singularity evolves in time the maximum height and concentration grow, and at $t \approx 3 \times 10^8$ the concentration exceeds the packing fraction. While this linear second-order diffusion may behave differently from the nonlinear fourth-order diffusion in (2.18), the unphysical concentrations suggest the model may be inaccurate for high concentrations.

3.4 Alternative Settling Function

In this section we propose a modification to the unregularized system (2.19) to ensure the concentration does not exceed ϕ_{max}. We begin with a heuristic explanation of how (2.12) may be incompatible with (2.1) in the limit $\phi \to \phi_{max}$. The volume-averaged velocity is controlled by $\mu(\phi)^{-1}$, which vanishes in this limit, while $f_{RZ}(\phi)$ and hence the relative flux is nonzero. This imposes a forward flux of particles with no net volume flux, requiring fluid therefore to move backward. This situation is probably unrealistic, because the limit $\mu(\phi) \to \infty$ is intended to model the case when the particles are packed tightly enough to prevent any shear flow. In that case, it seems more appropriate to model the particles as an immobile porous medium, with a Darcy's law flux of pure fluid and $\mathbf{v_{rel}} < 0$. Incorporating such a transition into the current model presents challenges, as the particle velocity must be specified relative to the laboratory frame rather than the fluid, essentially changing to a two-fluid model at high concentrations. A much simpler alternative is to simply let $\mathbf{v_{rel}}$ vanish along with $\mathbf{v}$ at $\phi = \phi_{max}$; this is readily accomplished by using the hindered settling function proposed by Buscall et al. [BGO82]

$$f_B(\phi) = (1 - \phi/\phi_{max})^5 \tag{3.12}$$

instead of (2.12). The two settling functions are plotted in figure 3.6.
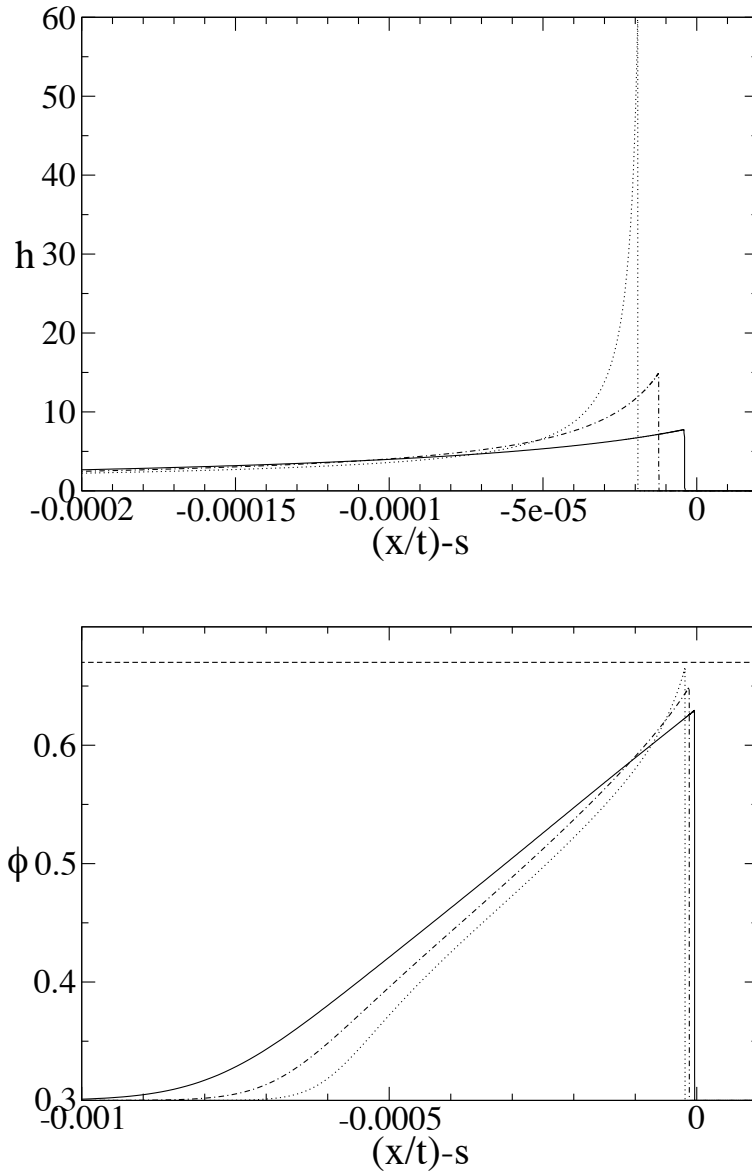
Figure 3.5: Film thickness (top) and particle concentration (bottom), from numerical solutions of the regularized system (3.6) in the singular shock regime, with $b = 0.001$, $\phi_0 = 0.3$, and $\epsilon = 1$, calculated on a grid moving at speed $s = 0.45547$ and evaluated at times 5×10^7 (solid), 1×10^8 (dot-dash), and 2×10^8 (dot). The dashed line on the bottom plot marks ϕ_m.

61
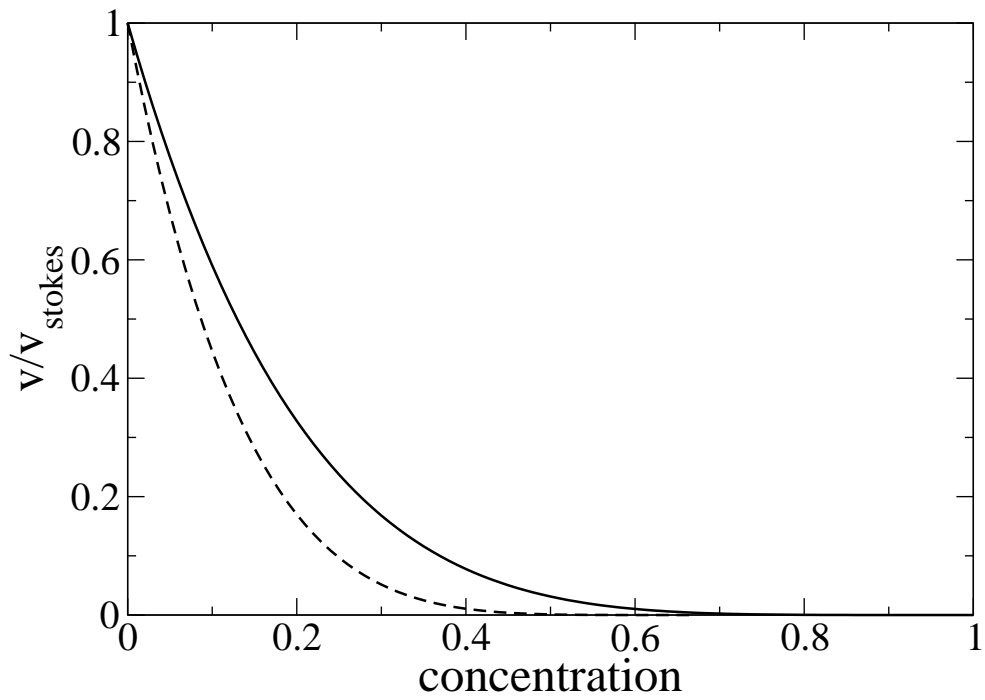
Figure 3.6: Two forms of the hindered settling function. The Richardson-Zaki form (solid line) vanishes at concentration 1.0, another form due to Buscall et al. (dashed line) vanishes at the packing fraction 0.67.

With this modification, solving the Riemann problem is simplified in two significant ways: the equations are strictly hyperbolic throughout the relevant domain Ω, and the bifurcation causing shock solutions to break down does not occur. In figure 3.7 we have plotted shock-shock connections for four values of b. These solutions exist even for very small precursors, so the system appears to be well-posed regardless of b. Figure 3.8 summarizes the manner in which the type of solution depends on the settling function and the Riemann data.

In figures 3.9-3.10, we compare the shock solutions to the two systems and their dependence on the precursor b. The behavior of the Hugoniot curves in the $f_{RZ}(\phi)$ system, shown in figure 3.2, implies the intermediate height and concentration approach a maximum value at a critical precursor thickness $b = b_* \approx 9 \times 10^{-4}$, below which there is no meaningful solution. As $b \to 0$ in the $f_B(\phi)$ system, the intermediate height increases apparently without bound and the concentration approaches ϕ_{max}. We also observed in both limits that the speeds of the 1- and 2- shocks to become approximately equal.

3.5   Genuine Nonlinearity

While most physical systems are strictly hyperbolic, systems arising naturally are often not genuinely nonlinear. In the Euler equations of compressible flow, one characteristic field is linearly degenerate: $r_i \cdot \nabla \lambda_i \equiv 0$. For this characteristic, $R_i(U)$ and $S_i(U)$ coincide and connections take the form of contact discontinuities, which satisfy (3.5) with the inequalities in (3.7) replaced by equality. More generally, when the variation of λ_i along R_i changes sign, the strict inequality in (3.7) becomes too restrictive and an entropy condition is needed to select which contact discontinuities are admissible solutions.
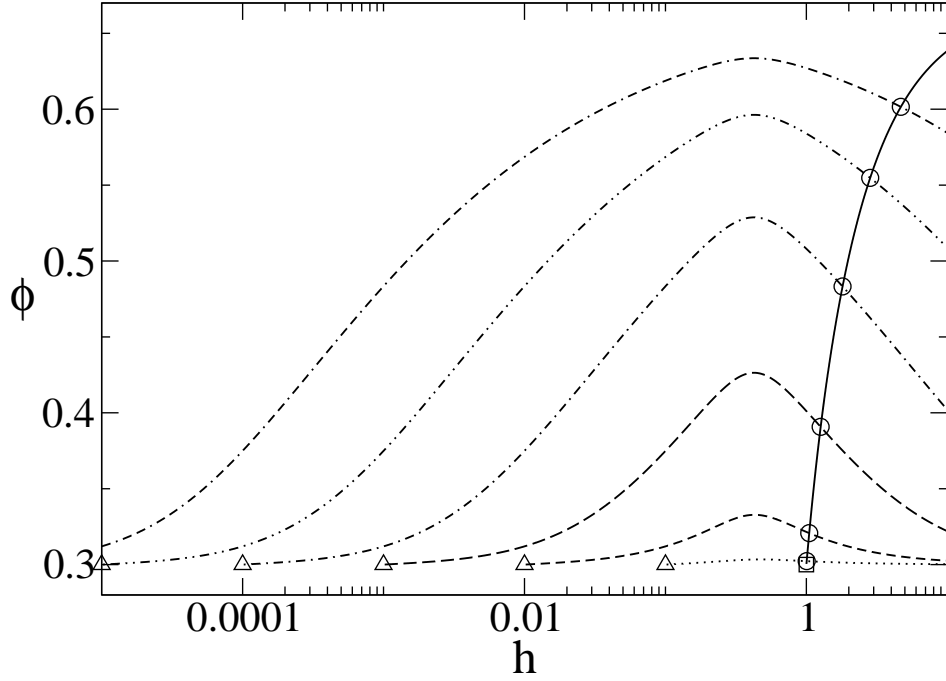
Figure 3.7: Shock connections using the settling function $f_B(\phi) = (1 - \phi/\phi_{max})^5$ instead of $f_{RZ}(\phi)$. The bifurcation that caused some initial data to have no solution no longer occurs. The solid line is the 1-shock connection from (h_L, ϕ_L), ($\square$), and the 2-shocks are plotted from various precursors ($\triangle$) given by $b = 10^{-1}$ (dot), 10^{-2} (short dash), 10^{-3} (long dash), 10^{-4} (dot-dash), 10^{-5} (dot-dot-dash), and 10^{-6} (dot-dash-dash). Each solution involves an intermediate state marked by $\bigcirc$.
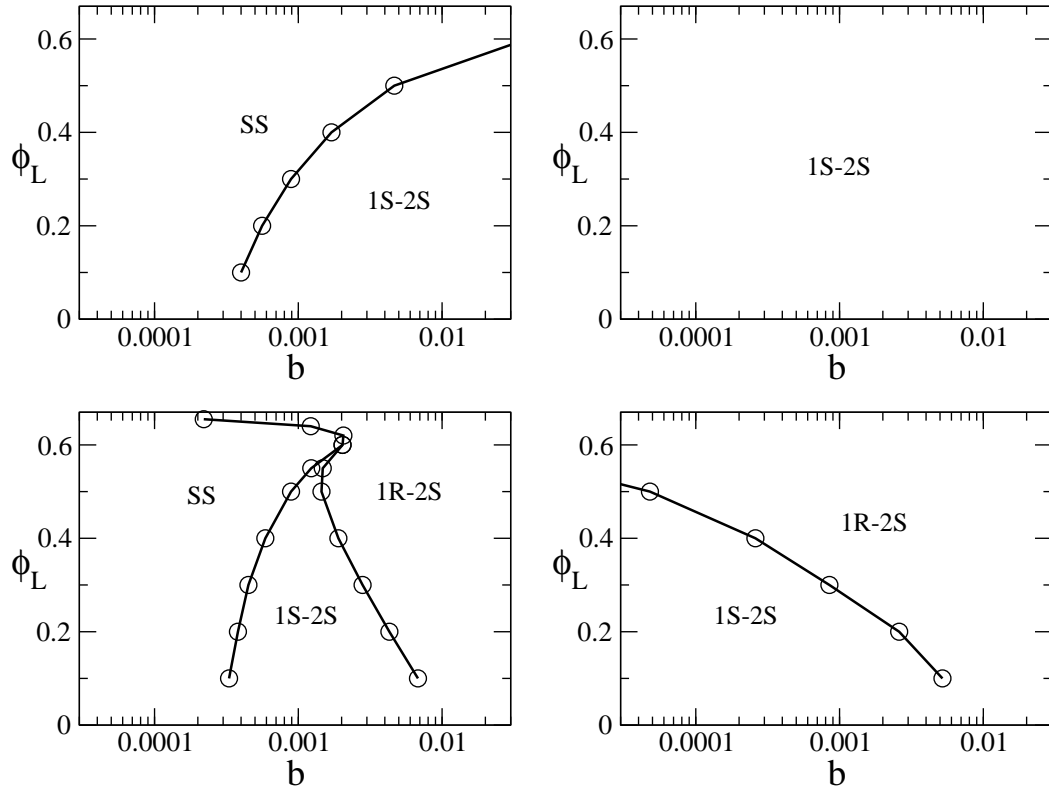
Figure 3.8: Type of solution (1-rarefaction and 2-shock, 1-shock and 2-shock, or singular shock) as determined by b and ϕ_L (assuming $h_L = 1$ and either $\phi_R = \phi_L$ or $\phi_R = 0$), for both hindered settling functions. Richardson-Zaki settling and $\phi_R = \phi_L$ (upper left), Richardson-Zaki settling and $\phi_R = 0$ (lower left), Buscall et al. settling and $\phi_R = \phi_L$ (upper right), Buscall et al. settling and $\phi_R = 0$ (lower right).
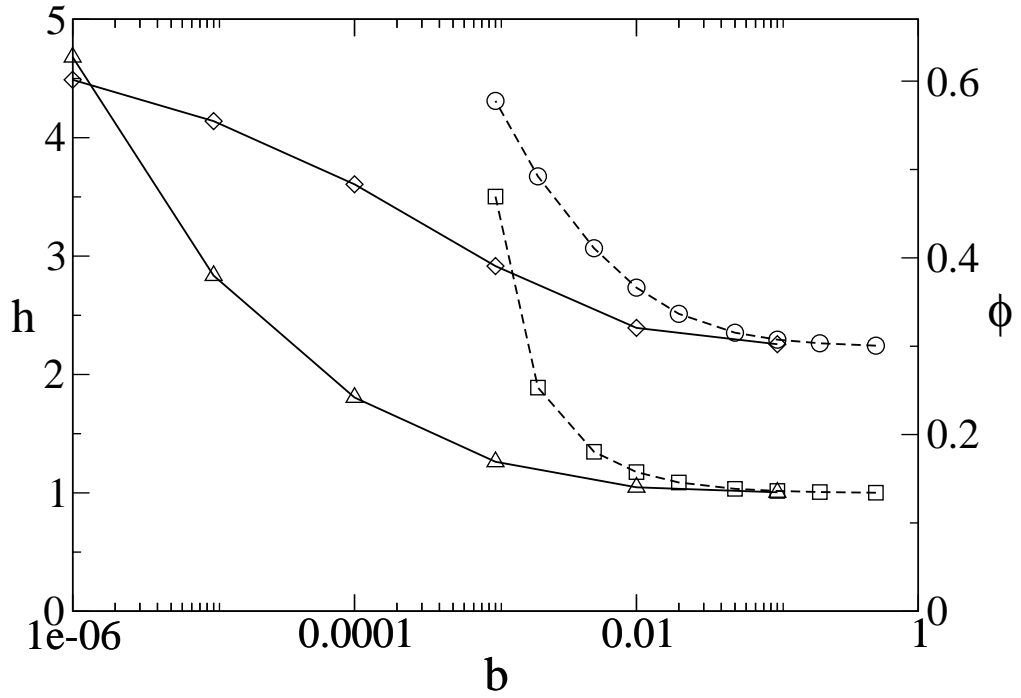
Figure 3.9: Height and concentration of the intermediate state vs. the precursor thickness b. Squares and circles are the height and concentration of solutions using the hindered settling function $f_{RZ}(\phi)$, triangles and diamonds are the height and concentration of solutions using $f_B(\phi)$.
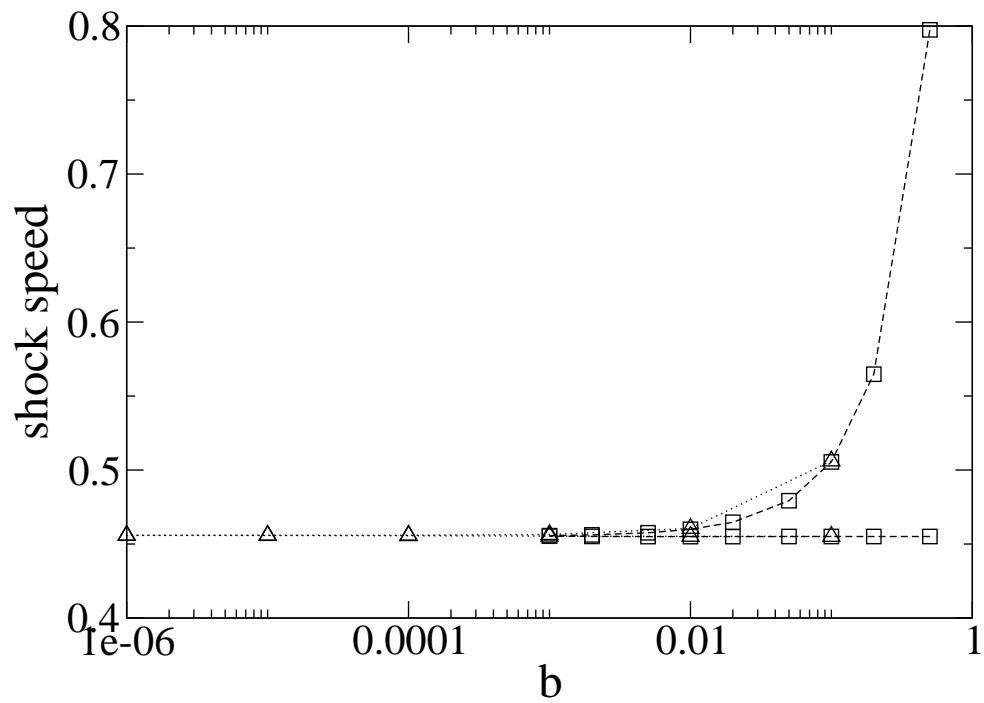
Figure 3.10: The speed of the shocks that make up the solutions to the connection problem for various precursors. Squares are solutions using the hindered settling function $f_{RZ}(\phi)$, and triangles with $f_B(\phi)$.

For a scalar conservation law, genuine nonlinearity is simply the strict convexity (or concavity) of the flux function F. If the function changes concavity, contact discontinuities are chosen by the Oleinik condition [Ole63], that the shock speed $s(U_L, U_R)$ satisfies

$$s(U_L, U_R) \leq s(U_L, U) \tag{3.13}$$

for any U between U_L and U_R. Liu has provided a generalization to 2×2 [Liu74] and $n \times n$ systems [Liu75] that requires (3.13) hold for all $U \in H(U_L)$ between U_L and U_R. Both Liu's and Oleinik's conditions reduce to (3.7) for a genuinely nonlinear system. While potentially only a bounded segment of $H(U_L)$ could be available for discontinuous waves, relaxing condition (3.7) provides more solutions by allowing both continuous and discontinuous waves in the same characteristic. Liu provides an existence proof, by constructing such a compound wave. This connection involves a shock to the first point U_* satisfying $s(U_L, U_*) = \lambda_i(U_*)$, followed by a rarefaction from U_* to $U_R \in R_i^+(U_*)$. The point U_* is both the first local minimum of s along $H(U_L)$, hence the last point for which Liu's entropy condition is satisfied, and the first point for which $\lambda_i \geq s$, necessary for a continuing rarefaction wave.

In (2.19), $r_1 \cdot \nabla \lambda_1 = 0$ holds along the curve shown in figure 3.11. For $(h_L, \phi_L) = (1, 0.3)$ the branches S_1^+ and R_1^- nearly coincide, so this branch represents to good approximation the states accessible through a 1-shock, 1-rarefaction compound wave as well. In figure 3.12 the eigenvalue and shock speed are plotted on this curve as a function of ϕ. For $\phi < \phi_L$, both speeds increase away from U_L, indicating a simple rarefaction. With $\phi_L < \phi_* \approx 0.369$, the shock speed is strictly decreasing with ϕ so the connection is a shock satisfying the Liu-Oleinik condition. This case includes the solutions described in §3.2 for $b = 0.1$ and $b = 0.01$. For $\phi > \phi_*$ neither simple wave is feasible, but a contact discontinuity
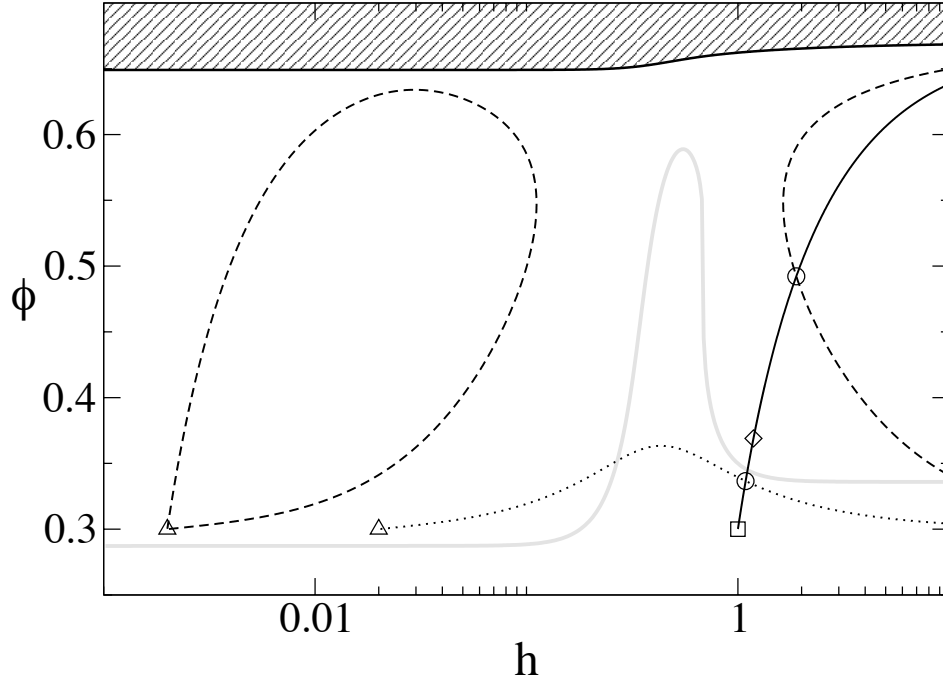
Figure 3.11: Failure of genuine nonlinearity for (2.19): $\nabla\lambda_1 \cdot r_1 = 0$ on the gray line. Connections from $(h_L, \phi_L) = (1.0, 0.3)$ ($\square$) are plotted on the dashed line, which include shocks up to $(h_*, \phi_*) \approx (1.18, 0.369)$ ($\diamond$) or a compound shock to (h_*, ϕ_*) followed by a rarefaction. 2-shocks are plotted from right states ($\triangle$) for one case ($b = 0.02$, dotted line) with a simple 1-shock, 2-shock solution, and another case ($b = 0.002$, dashed line) with a compound 1-shock, 1-rarefaction wave and a 2-shock. The equations are elliptic in the shaded region.
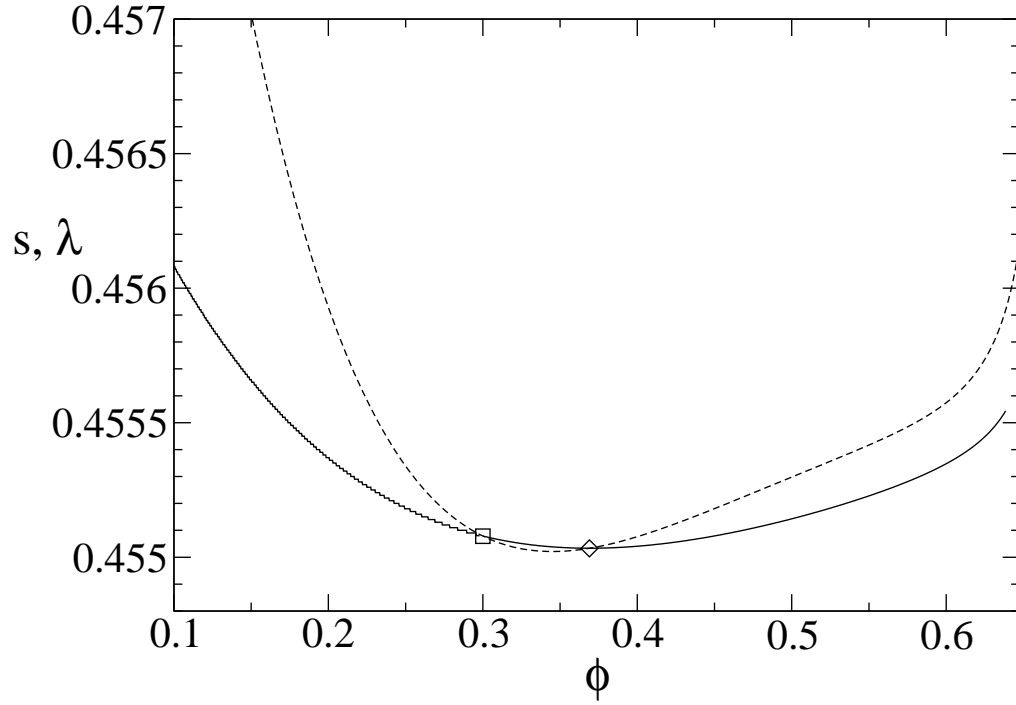
Figure 3.12: Rarefaction speeds (dashed line) and shock speeds (solid) for the connections along the first characteristic from a left state $(h_L, \phi_L) = (1.0, 0.3)$, ($\square$), (corresponding to figure 3.1), plotted as a function of the concentration ϕ_R at the right state. The linear degeneracy curve in figure 3.11 indicates the minimum characteristic speed occurs at $\phi_R \approx 0.34$. If $\phi_R > \phi_* \approx 0.37$ ($\diamondsuit$), a single shock solution is not admissible and the solution consists of a hybrid shock-rarefaction wave.

from ϕ_L to ϕ_* can connect with a rarefaction from ϕ_* to ϕ because λ_1 is now both increasing and greater than the shock speed.

This compound wave is in practice difficult to distinguish from a simple shock. As noted above, the states accessible to a compound wave are nearly the same states lying on R_1 or S_1, so the constant state U_I appearing between 1-waves and 2-waves cannot easily be used to identify the compound wave. Additionally, figure 3.12 demonstrates that λ_1 changes very slowly along its characteristic at intermediate concentrations, so for instance in the presence of numerical diffusion, the rarefaction appears indistinguishable from a shock. Thus although some solutions are necessarily compound waves, their observable properties (other than failing to satisfy the Lax condition) are similar to those of a simple shock.

CHAPTER 4

Linear Stability of the Contact Line

This chapter characterizes the stability of the contact line of a particle-laden film in the context of the lubrication model described above, with respect to the transverse perturbations that may grow into the fingering instability. The important result is a linear stability analysis performed by Dr. Oleg Alexandrov, which provides a theoretical explanation for Zhou et al.'s observation that the particle-rich ridge suppresses the instability. The basic mechanism is understood from the clear fluid case, in which the destabilizing effect of the fluid velocity increasing with film thickness competes with the stabilizing effect of surface tension. The involvement of surface tension indicates that the full fourth-order equations (2.17) need to be studied in any stability calculation. In dimensionless form, the two-dimensional system then appears as

$$
h_t + \nabla \cdot \left\{ \frac{h^3}{\mu(\phi)} \nabla \nabla^2 h - D(\alpha) \left[\frac{h^3}{\mu(\phi)} \nabla(\rho(\phi)h) - \frac{5}{8} \frac{h^4}{\mu(\phi)} \nabla(\rho(\phi)) \right] \right\} + \left\{ \frac{\rho(\phi)}{\mu(\phi)} h^3 \right\}_x = 0
$$

(4.1)

$$
(\phi h)_t + \nabla \cdot \left\{ \frac{\phi}{\mu(\phi)} h^3 \nabla \nabla^2 h - D(\alpha) \left[\frac{\phi}{\mu(\phi)} h^3 \nabla(\rho(\phi)h) - \frac{5}{8} \frac{\phi}{\mu(\phi)} h^4 \nabla(\rho(\phi)) \right] \right\}
$$
$$
+ \left\{ \frac{\phi \rho(\phi)}{\mu(\phi)} h^3 + V_s \phi h f(\phi) w(h) \right\}_x = 0. \quad (4.2)
$$

Numerical simulations of equations (4.1)-(4.2) show an instability affecting ϕ but not h. This is because the second- and fourth-order regularizing terms,

although present in both equations, affect only the average velocity

$$\mathbf{v_{av}} = \frac{h^3}{\mu(\phi)}\nabla\nabla^2 h - D(\alpha)\left[\frac{h^3}{\mu(\phi)}\nabla(\rho(\phi)h) - \frac{5}{8}\frac{h^4}{\mu(\phi)}\nabla(\rho(\phi))\right] + \frac{\rho(\phi)}{\mu(\phi)}h^3\hat{\mathbf{x}}. \quad (4.3)$$

of the two phases, and not the relative velocity

$$\mathbf{v_{rel}} = V_s f(\phi)w(h)\hat{\mathbf{x}} \qquad (4.4)$$

of the particles with respect to the liquid. A stable two-dimensional model must include a regularizing effect on this relative velocity.

Such regularization should naturally be present due to shear-induced diffusion. Due to the thin geometry of film flow, diffusion will be most pronounced in the (normal) z direction, an effect already incorporated in the model in the assumption that particles are evenly distributed in this direction. As the detailed below, this effect can also be significant in horizontal directions when gradients in ϕ are large.

Leighton and Acrivos [LA87] describe shear-induced diffusion as a concentration- and shear rate-dependent diffusion of particles with diffusivity $D = a^2\dot{\gamma}\hat{D}(\phi)$ for a suspension subject to a shear rate $\dot{\gamma}$, and experiments of Leighton [Lei85] indicate that the dimensionless coefficient is approximated by $\hat{D}(\phi) = \frac{1}{3}\phi^2\left(1 + \frac{1}{2}e^{8.8\phi}\right)$.

Using dimensional variables, the particle flux due to shear induced migration appears as an extra term in equation (4.4):

$$(\phi h)_t + \nabla\cdot\left((\mathbf{v_{av}} + \mathbf{v_{rel}})\phi h - \left[a^2\dot{\gamma}\hat{D}(\phi)\right]h\nabla\phi\right) = 0. \qquad (4.5)$$

The shear rate can be approximated by $\dot{\gamma} = |d\mathbf{v_{av}}/dz|$. In smooth regions this velocity is generally dominated by its first order term, which before depth-averaging is

$$\mathbf{v_{av}}(z) \approx \frac{3\rho(\phi)}{\mu(\phi)}\left(hz - \frac{z^2}{2}\right), \qquad (4.6)$$

giving an average shear rate

$$\dot{\gamma} \approx \frac{3}{2}(g\sin\alpha)\frac{\rho(\phi)}{\mu(\phi)}h. \tag{4.7}$$

Substituting (4.7) and the velocities (4.4)-(4.3) into (4.5) and reverting to dimensionless variables then yields the equation

$$(\phi h)_t + \nabla \cdot \left\{ \frac{\phi}{\mu(\phi)}h^3\nabla\nabla^2 h - D(\alpha)\left[\frac{\phi}{\mu(\phi)}h^3\nabla(\rho(\phi)h) - \frac{5}{8}\frac{\phi}{\mu(\phi)}h^4\nabla(\rho(\phi))\right] \right.$$
$$\left. -\frac{3}{2}a^2(3Ca)^{1/3}\hat{D}(\phi)\frac{h^2\rho(\phi)}{\mu(\phi)}\nabla\phi \right\} + \left\{ \frac{\phi\rho(\phi)}{\mu(\phi)}h^3 + \frac{2}{3}V_s\phi h f(\phi)w(h) \right\}_x = 0 \quad (4.8)$$

for the particle flux, replacing equation (4.2), while equation (4.1) remains unaltered.

The base state for a contact line stability analysis is the solution to the system (4.1), (4.8) with one-dimensional Riemann initial data:

$$h(x, y, t = 0) = \begin{cases} 1 & \text{for } x < 0 \\ b & \text{for } x > 0 \end{cases} \tag{4.9}$$

$$\phi(x, y, t = 0) = \phi_0 \tag{4.10}$$

representing the opening of a gate along the line $x = 0$ at time $t = 0$, which admits a film of depth 1 and concentration ϕ_0 onto a dry surface and assumes a precursor film of thickness $b \ll 1$. A numerical solution of this base state calculated by Oleg Alexandrov is shown in figure 4.1, along with a numerical solution of the reduced system (2.19). As reported in [ZDB05], the reduced system remains a good approximation of the full fourth-order system, differing primarily in the lack of a capillary ridge, so the first-order shock terminology remains a useful way to describe solutions of the fourth-order system.

In two dimensions, the regularized shock solution corresponds to a straight contact line. Whether the contact line remains straight in any experiment is
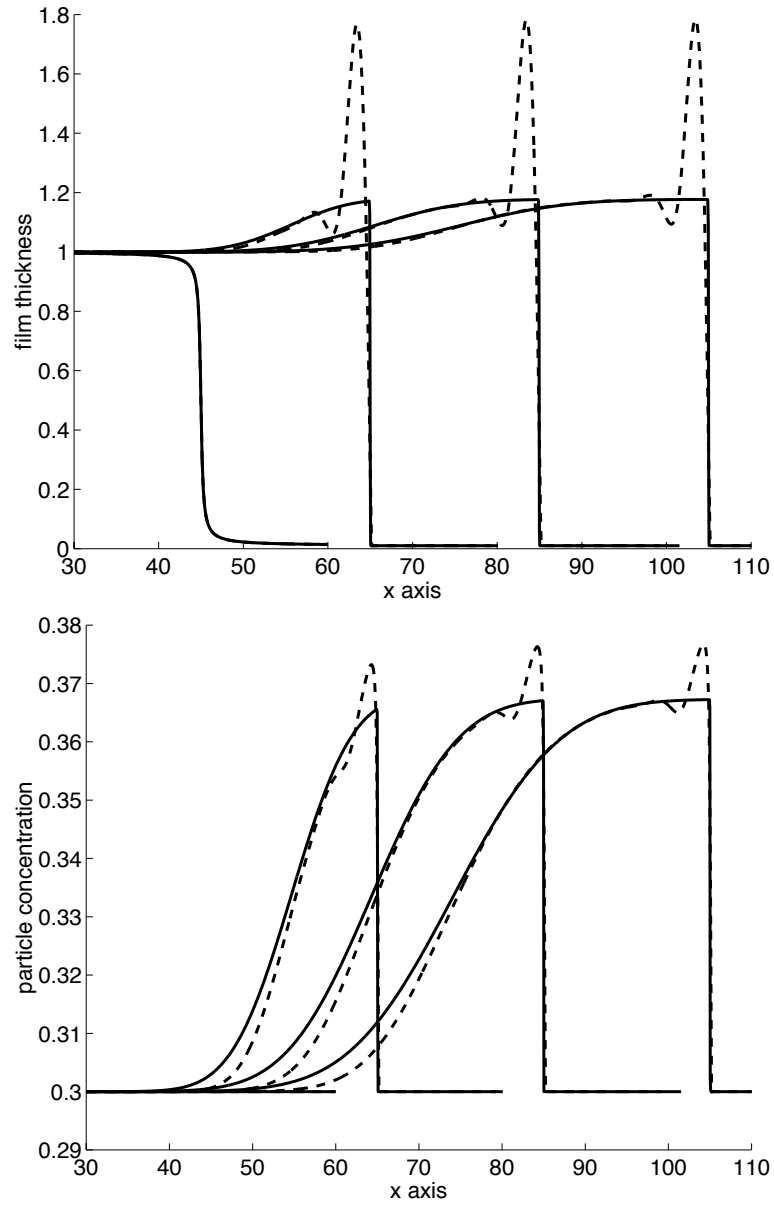
Figure 4.1: The base state, obtained by a numerical solution of the one-dimensional Riemann problem at times 0, 2000, 4000, and 6000. Dashed lines are solutions of the full fourth-order equations and solid lines are shock solutions of the first-order reduced system. The smoothness of the trailing shock is a numerical artifact. The left plot displays film thickness, and the right is concentration. The simulation parameters are as follows: $\phi_0 = 0.3$, $b = 0.01$, $\alpha = \pi/2$. The graphs have been shifted along the x axis to make them appear closer together.

determined by the stability of this base state with respect to transverse perturbations. In the clear fluid problem, the base state is a single regularized shock and can be written as a traveling wave $h(x,t) = h(x - Ut)$ for an appropriate choice of U [THS89, BB97]. In contrast a double shock solution cannot be represented as a traveling wave, so in this case the base state must be considered a function of both x and t.

Following [BSB05], the dynamic linear stability analysis begins with the ansatz

$$\bar{h}(x,y,t) = h(x,t) + \varepsilon g(x,t)\cos qy \tag{4.11}$$

$$\bar{\phi}(x,y,t) = \phi(x,t) + \varepsilon\psi(x,t)\cos qy, \tag{4.12}$$

which allows, together with equations (4.1) and (4.8), the derivation of the following evolution equations for the perturbations g and ψ:

$$g_t + \left\{ h^3 \left[a(\phi)\left(g^{(3)} - q^2 g'\right) + a'(\phi)h^{(3)}\psi \right] + 3a(\phi)h^2 h^{(3)}g \right\}_x + q^2 a(\phi)h^3\left(q^2 g - g''\right)$$

$$+ \left\{ h^2 \left[3b(\phi)g + hb'(\phi)\psi \right] \right\}_x = 0 \quad (4.13)$$

$$(\phi g + h\psi)_t + \left\{ h^3 \left[c(\phi)\left(g^{(3)} - q^2 g'\right) + c'(\phi)h^{(3)}\psi \right] + 3c(\phi)h^2 h^{(3)}g \right\}_x + q^2 c(\phi)h^3\left(q^2 g - g''\right)$$

$$+ \left\{ h^2 \left[3d(\phi)g + hd'(\phi)\psi \right] \right\}_x$$

$$+ V_s \left\{ f(\phi)w(h)\left[\phi g + h\psi\right] + h\phi\left[\psi w(h)f'(\phi) + f(\phi)gw'(h)\right] \right\}_x$$

$$- C \left[\left\{ p'(h)r(\phi)\phi_x g + p(h)r'(\phi)\phi_x\psi + p(h)r(\phi)\psi_x \right\}_x - q^2 p(h)r(\phi)\psi \right] = 0. \quad (4.14)$$

Here we denoted $a(\phi) = 1/\mu(\phi)$, $b(\phi) = \rho(\phi)/\mu(\phi)$, $c(\phi) = \phi/\mu(\phi)$, $d(\phi) = \phi\rho(\phi)/\mu(\phi)$, $C = \frac{3}{2}a^2(3Ca)^{1/3}$, $p(h) = h^2$, $r(\phi) = \hat{D}(\phi)\rho(\phi)/\mu(\phi)$. Also, for simplicity, it is assumed that the film flows vertically so $\alpha = \pi/2$ and $D(\alpha) = 0$.

Sufficiently small perturbations will grow or decay exponentially in time, i.e. as $e^{\beta(q)t}$. Anticipating this behavior, the growth rate $\beta(q)$ was extracted from
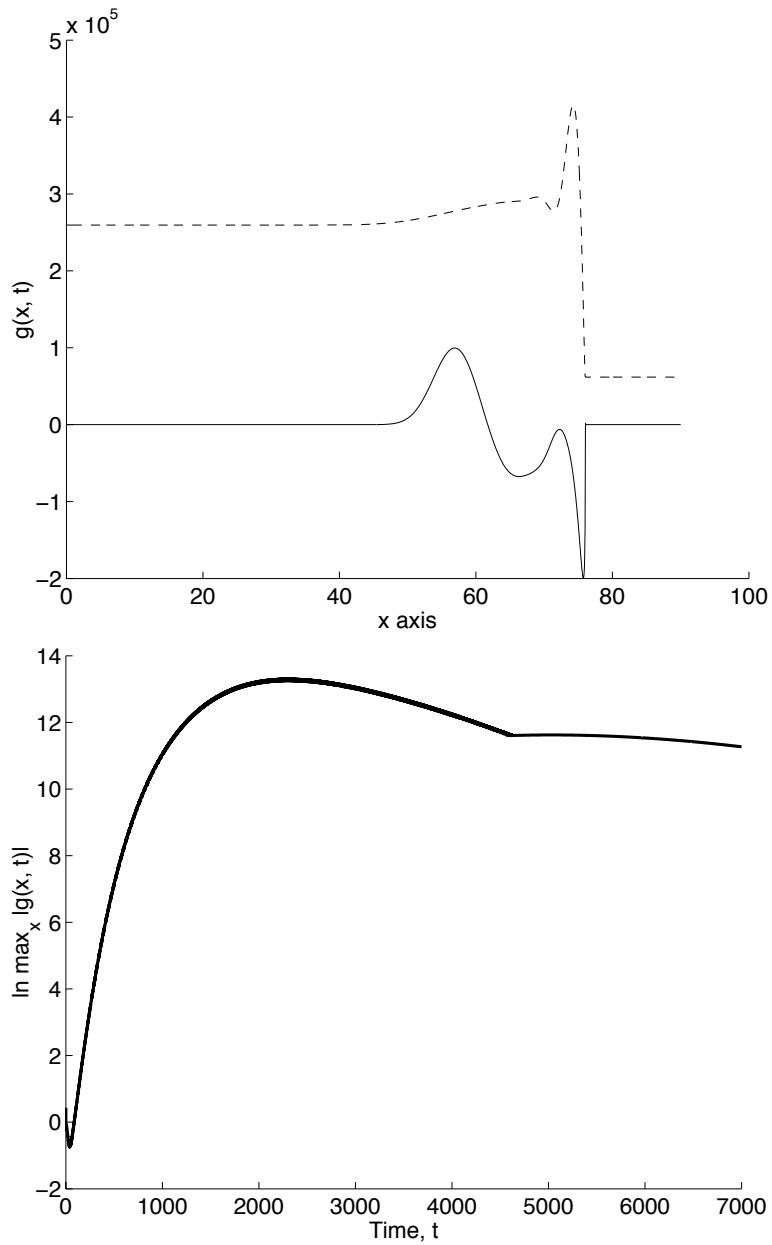
Figure 4.2: On the left, the perturbation $g(t, x)$ at time $T = 4000$ for $q = 1$ (the solid line). The superimposed dashed curve is $h(x, t)$ shown to illustrate the positions of the leading and trailing shocks. On the right is the decay of the perturbation in time. Around $T = 4000$ the part of the perturbation at the trailing shock starts dominating the part of the perturbation at the leading shock, and the decay slows down. The parameters used are $b = 0.01$, $\phi_0 = 0.3$, $\alpha = \pi/2$.

numerical simulations of the perturbation equations (4.13)-(4.14) by examining the evolution of the quantity $\max_x |g(t, x)|$ in time. An example of this evolution appears in figure 4.2, showing a complication that occurs as the perturbation splits into two parts, each localized near one of the shocks. At early times the maximum is attained by the perturbation at the leading shock, but later the perturbation at the trailing shock dominates, and this transition shows up as a kink in the amplitude plot.

The long time growth rates were used to infer $\beta(q)$, shown in figure 4.3, which like the pure fluid case displays a long wave instability. Also plotted are the growth rates from calculations with V_s set to zero, which forces the concentration to remain constant, thereby modeling a homogeneous fluid with the same bulk properties as the mixture. The differences in the growth rate between the two calculations can then be attributed to settling and the associated particle-rich ridge, and this effect appears as an 11% reduction in the growth rate of unstable modes.

The above stability analysis shows that particle settling and the formation of a ridge has a moderate stabilizing effect, slowing the growth rate of the fingering instability and pushing the most unstable mode to a slightly longer wavelength. This matches the effect seen in the experiments of Zhou et al. [ZDB05], though it is not clear that the modest reduction in the growth rate described above is sufficient to explain the observed effect on finger growth.
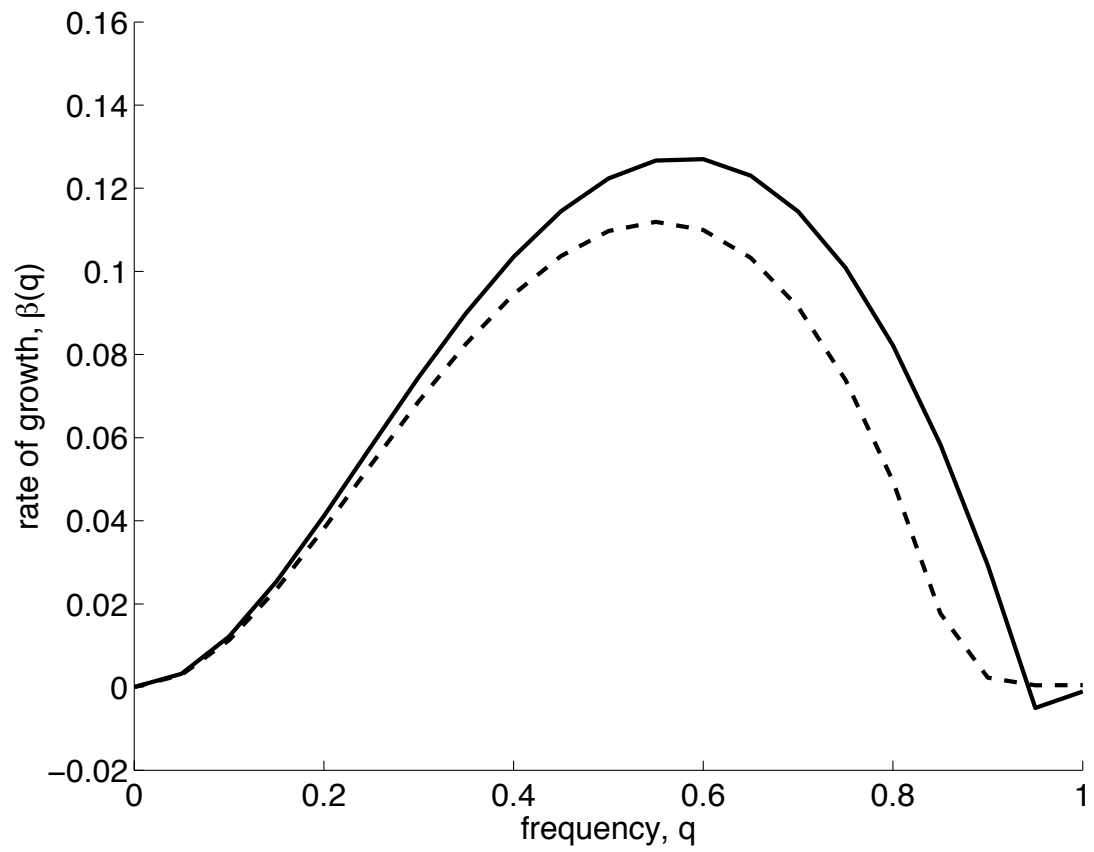
Figure 4.3: The growth rate $\beta(q)$ for the film without settling (solid) and with settling (dash).

CHAPTER 5

Shear Induced Migration in a Thin Film

This chapter analyzes the effects of shear-induced migration on the vertical distribution of particles in a film. The models presented above assumed this is always a uniform distribution, but for more accuracy the distribution should determined by a balance between migration and gravity.

Such a balance has been calculated before by Schaflinger et al. [SAZ90] and by Timberlake and Morris [TM05]. Shaflinger et al. used the "diffusive flux" model for shear-induced diffusion introduced by Leighton and Acrivos [LA87], which states that the volume flux of particles is given by

$$N_d = -a^2 \dot{\gamma} \hat{D}(\phi) \nabla \phi, \tag{5.1}$$

where $\dot{\gamma}$ is the shear rate, a is the particle radius, and the dimensionless diffusion coefficient was found by Leighton [Lei85] to be well approximated by $\hat{D}(\phi) = \frac{1}{3}\phi^2(1 + \frac{1}{2}e^{8.8\phi})$. The use of the scalar shear rate restricts this model to simple shear flows, such as one-dimensional film flow where $\dot{\gamma} = dv/dz$ and v is the velocity of the mixture. Schaflinger et al. balanced this flux with that due to gravitational settling in the z direction, which they approximated with a hindered settling function. This condition along with the Newtonian stress balance allowed them to derive a system of two first-order ordinary differential equations for the concentration and shear stress, which they solved numerically.

Two important features of the solutions can be deduced from the form of (5.1).

The diffusive flux must be always directed upward in order to balance gravity, which implies by (5.1) that $d\phi/dz \leq 0$. Also, since the flux is proportional to the shear rate, the vanishing stress at the free surface $z = h$ ensures there is no diffusive flux to balance settling, and therefore $\phi(h) = 0$ for all solutions[1].

Timberlake and Morris included theory for the depth profile of concentration in their experimental paper on film flow of a neutrally buoyant suspension. Their description uses the "suspension balance" model of Nott and Brady [NB94] for particle migration. That more rigorous model calculates a "temperature" measuring fluctuations in particle velocities, which is generated by shear, dissipated by viscous stress, and diffuses through an effect related to the finite particle size. This last property is the most significant difference between the diffusive flux and suspension balance models, implying that particle migration depends nonlocally on the shear rate, which in this case allows a small nonzero concentration at the free surface. Otherwise the two models generally give similar predictions [FMB02]. Since Timberlake and Morris considered neutrally buoyant particles, ϕ increases with z, which is also confirmed by their experiment. Rather than assuming the film is always in diffusive equilibrium, they retain the x coordinate in the flow direction, and their calculations indicate a distance on the order of $200h$ is necessary to reach equilibrium. This factor decreases strongly with the bulk concentration and is proportional to $(h/a)^2$.

5.1   Derivation of the Model Equations

This analysis will use diffusive flux model for simplicity, and proceed similarly to Schaflinger et al., but differ crucially by using an extra term in which the particle

---

[1]A steady solution with no diffusive flux is also possible where the maximum concentration ϕ_m is reached, corresponding to packed spheres, however this cannot happen at the free surface in Shaflinger et al.'s model because $d\phi/dz \leq 0$.

flux opposes gradients in the shear rate, in addition to opposing concentration gradients as in (5.1). Here we use the particle migration expression [PAB92] (1.25) rewritten as

$$\frac{D\phi}{Dt} = a^2 \nabla \cdot \left[K_c \phi \nabla(\dot{\gamma}\phi) + K_\eta \dot{\gamma} \frac{\phi^2}{\mu(\phi)} \nabla \mu(\phi) \right],$$

(5.2)

with the values $K_c = 0.43$ and $K_\eta = 0.65$ for the two constants. Equation (5.2) corresponds to a particle flux

$$
\begin{aligned}
F_m &= -a^2 K_c \phi \nabla \left(\frac{\sigma}{\mu(\phi)} \phi \right) - a^2 (K_\eta - K_c) \frac{\sigma \phi^2}{\mu(\phi)^2} \nabla \mu(\phi) \\
&= -\frac{a^2 \phi}{\mu(\phi)} \left(K_c \nabla(\sigma\phi) + (K_\eta - K_c) \frac{\sigma\phi}{\mu(\phi)} \nabla \mu(\phi) \right),
\end{aligned}
$$

(5.3)

where the shear rate $\dot{\gamma}$ has been eliminated in favor of the shear stress $\sigma = \mu(\phi)\dot{\gamma}$.

For a flat film on an incline, equilibrium is reached when this flux balances that of gravitational settling in the z direction, which will again be modeled using a hindered settling function. In this case it is convenient to follow Schaflinger et al. and use the hindered settling function $f(\phi) = (1 - \phi)/\mu(\phi)$, leading to the settling flux

$$F_s = -\frac{2}{9} \frac{a^2 \Delta \rho g \cos \alpha}{\mu_f} \frac{\phi(1 - \phi)}{\mu(\phi)}.$$

(5.4)

The balance of flux $F_m + F_s = 0$ then takes the form

$$K_c(\sigma\phi)' + (K_\eta - K_c) \frac{\sigma\phi}{\mu(\phi)} \mu(\phi)' = -\frac{2}{9} \frac{\Delta \rho g \cos \alpha}{\mu_f} (1 - \phi)$$

(5.5)

where the gradients have been replaced primes denoting differentiation by z. Substituting the viscosity formula $\mu(\phi) = \mu_f(1 - \phi/\phi_m)^{-2}$ and differentiating yields

$$
\begin{aligned}
&\left[1 + \frac{2(K_\eta - K_c)}{K_c} \frac{\phi}{\phi_m - \phi} \right] \sigma\phi' \\
&= \phi(1 + \Delta\phi) - \frac{2\Delta}{9K_c} (\cot \alpha)(1 - \phi),
\end{aligned}
$$

(5.6)

82

where z and σ have now been nondimensionalized using the depth of the film h and the unit of stress $(\rho g/h)\sin\alpha$.

For a flat film there is no curvature, so the pressure can be set to zero at the free surface $z = 1$, and is simply hydrostatic in the suspension. The nondimensional shear stress then satisfies the equation

$$\sigma' = -(1 + \Delta\phi). \tag{5.7}$$

Equations (5.6) and (5.7) constitute the system to be studied here, with the understanding that (5.6) is replaced by $\phi' = 0$ when $\phi = 0$ or $\phi = \phi_m$ to ensure pure fluid and packed particles are admissible solutions and to keep the concentration within its meaningful range. The physical boundary conditions both involve the stress: $\sigma(0) = (1 + \Delta\phi_0)$ and $\sigma(1) = 0$, where ϕ_0 is the imposed average concentration. Thus for these two equations there is only a one-parameter family of physically meaningful solutions, parameterized by ϕ_0. In practice this system was easiest to solve by shooting with a Runge-Kutta method from $z = 0$ while adjusting the value of $\phi(0)$. Once σ and ϕ are determined, the mixture velocity can be calculated using $dv/dz = \dot{\gamma} = \sigma(z)/\mu(\phi(z))$ and $v(0) = 0$.

5.2 Solutions

Since particle migration in this model does not strictly oppose the concentration gradient, ϕ is not constrained to decrease with z as in the work of Schaflinger et al. The lack of a migration flux at the free surface however is general to the diffusive flux model, and still applies here, forcing either $\phi(1) = 0$ or $\phi(1) = \phi_m$. Since $\sigma \geq 0$, it is also apparent from equation (5.6) that $\phi(z)$ is monotone, since $\sigma\phi'$ is determined by a function of ϕ only with a single unstable root $\phi^* = \phi^*(\alpha)$ in its allowable domain (between 0 and ϕ_m). There are then two possibilities:

$\phi_0 > \phi(0) > \phi^*$ with $\phi(1) = \phi_m$, or $\phi_0 < \phi(0) < \phi_m$ with $\phi(1) = 0$.

Considering the latter case, the particulate phase is located preferentially near the bottom of the film and (because $v(z)$ is always increasing) moves slower than the fluid on average, both of which are necessary conditions for the particles to settle out of the flow. It seems natural then to associate $\phi_0 < \phi^*(\alpha)$ with this regime in Zhou et al.'s experimental work [ZDB05]. The case $\phi_0 > \phi^*(\alpha)$ should then correspond to the particle-rich ridge regime, as the particles do not settle to the bottom and move faster on average than the fluid, even without including the settling velocity in the flow direction. While there is no obvious reason why there should be a regime (other than the single solution $\phi \equiv \phi^*$) where the fluid and particles move at the same velocity, it may be that experiments in which the suspension stayed well-mixed had $\phi_0 \approx \phi^*$ and the relatively small difference between the two velocities did not have time to produce noticeable segregation on the experimental time scale. Plotted in figure 5.1 is the curve $\phi^*(\alpha)$ overlayed on the experimental data of Zhou et al., which appears consistent with this hypothesis.

Figure 5.2 shows the concentration and velocity profiles for two solutions of this system at $\alpha = 45°$ with $\phi^*(\alpha) = 0.35$, for $\phi_0 = 0.45$ and $\phi_0 = 0.25$. The effect of increasing concentration for $\phi_0 = 0.45$ is to flatten the velocity profile near the top from the parabolic shape of an unstratified film, while for $\phi_0 = 0.25$ the velocity has an inflection point in this area. Also of interest is the fact that when $d\phi/dz > 0$ both phases move faster than the velocity of an unstratified film, because of the high-shear, low-ϕ region at the bottom and the low shear at the top where v is at its greatest. Both phases are slower when $d\phi/dz < 0$.

In figure 5.3 the relative velocity due to stratification is compared with the in-plane settling velocity used in [ZDB05] and [CBH06] at $\alpha = 45°$. Specifically
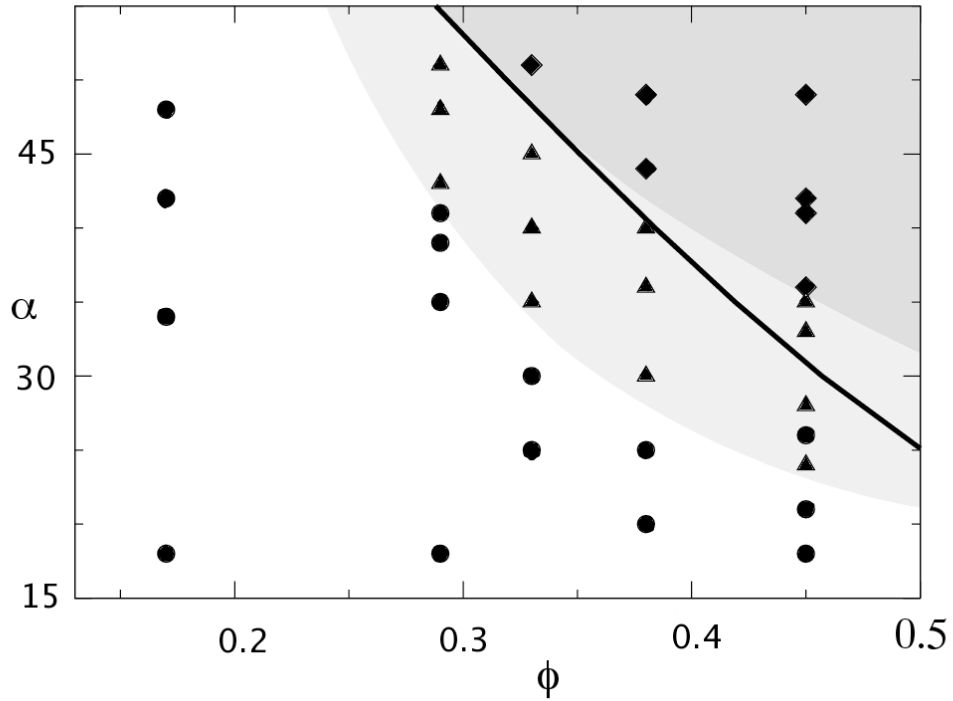
Figure 5.1: The function $\phi^*(\alpha)$ determining whether particles concentrate toward the top or bottom of the film, overlaid on Zhou et al.'s experimental parameters for which particles settle to the substrate (circle, white region), remain well mixed (triangle, light region), and accumulate in a ridge (diamond, dark region). Experimental data were inferred from figure 2 of [ZDB05].
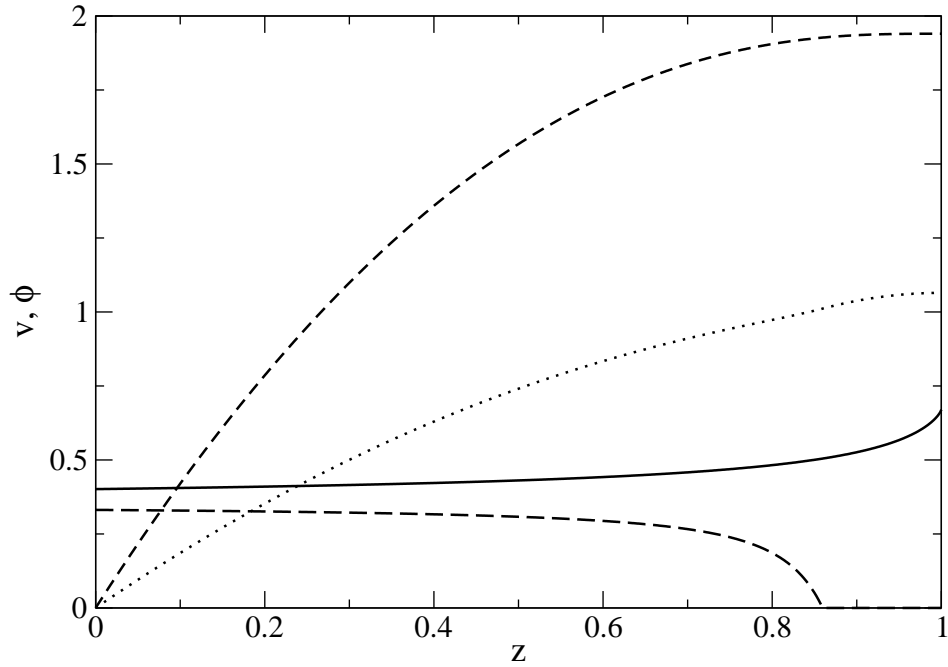
Figure 5.2: Depth profiles of ϕ and v for two average concentrations at $\alpha = 45°$. Bulk concentration $\phi_0 = 0.25$: velocity (dot) and concentration (long dash), bulk concentration $\phi_0 = 0.45$: velocity (short dash) and concentration (solid). Velocities are scaled by the average velocity of a homogeneous film at the same concentration. With this rescaling the average velocities at $\phi_0 = 0.25$ of the particle and liquid phases are 0.57 and 0.70, and at $\phi_0 = 0.45$ the velocities are 1.41 and 1.33 respectively.
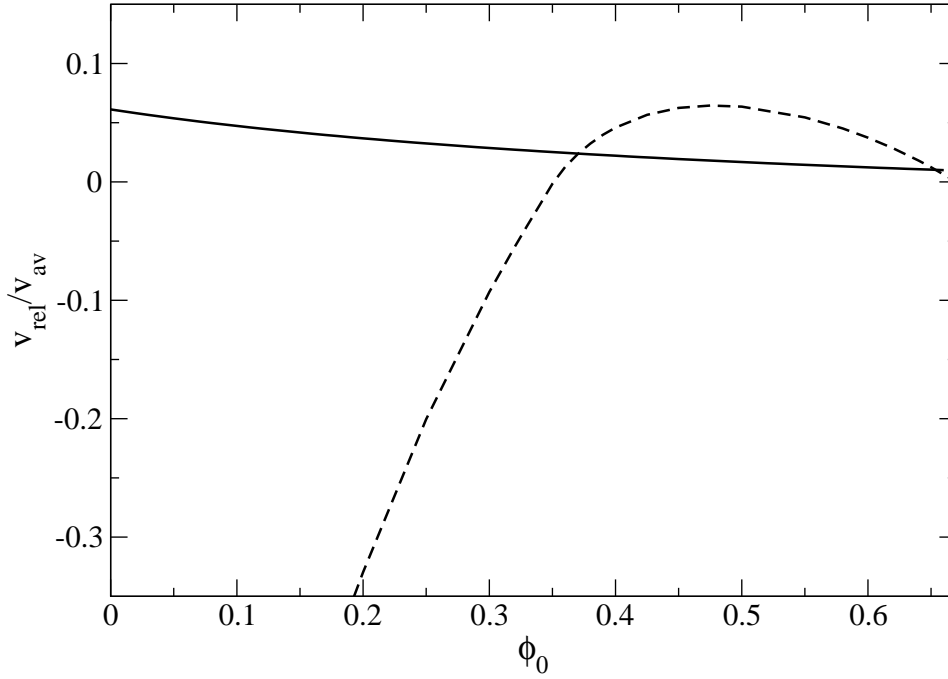
Figure 5.3: The ratio $v_{rel}/v_{av} = (v_p - v_f)/(\phi v_p + (1 - \phi)v_f)$ of velocities relevant for formation of the particle rich ridge. Velocity difference due to the stratified flow as described above (dash), and velocity difference due to direct gravitational settling in the flow direction as described by Zhou et al. (solid).

the vertical axis measures the ratio $v_{rel}/v_{av} = (v_p - v_f)/(\phi v_p + (1 - \phi)v_f)$ that determines the accumulation of particles in an experiment limited by the length of the channel. For concentrations greater than 0.37, stratification has a larger effect than in-plane settling. Since the particle-rich ridge occurs at rather high concentrations, the stratified flow appears to be the more important cause of the ridge.

A description of the ridge regime including stratification is possible within the lubrication context if the film is assumed to be always in equilibrium between settling and migration, by using the calculations of figure 5.3 to determine the relative velocity from ϕ. This assumption does not appear to be justified, however, especially since the solution can be expected to develop shocks as in [CBH06], so a fully two-dimensional model may be necessary. The experiments and two-dimensional calculations of Timberlake and Morris [TM05] indicate the distance travelled before reaching this equilibrium is on the order of tens of centimeters, even for an experiment with somewhat larger particles such as Zhou et al. [ZDB05]. Non-equilibrium effects would probably not alter the selection of settling regimes other than to increase the time for which the film stays well-mixed, making that regime more likely for length-limited experiments.

CHAPTER 6

Summary

In chapter 1 we reviewed the literature on thin films, focusing on those studies most relevant to this work. Studies of thin films have dealt with the rate of advance, which in lubrication theory is determined by the shape of the free surface, and with the fingering instability that often deforms the contact line. Special modeling techniques are needed to deal with the advancing contact line, because lubrication models give unphysical results at the contact line. We reviewed several studies of suspension flow, demonstrating the use of common continuous models for particle settling, effective viscosity, and shear-induced migration. We also discussed the experiments by Zhou et al. of particle-laden films[ZDB05], which posed the problems that this dissertation addresses: the appearance of a particle-rich ridge and its effect on the contact line instability, and the selection between this ridge and two other settling behaviors.

In chapter 2 we derived a lubrication model consisting of two fourth-order equations for particle-laden film flow, incorporating effective viscosity and horizontal particle settling. This derivation follows the procedure outlined in [ZDB05], and produces a corrected system that is also generalized to two dimensions.

Chapter 3 follows the technique suggested in [ZDB05] of analyzing the reduced system, obtained by neglecting second- and fourth-order spatial derivatives, which takes the form of a 2×2 system of conservation laws. The theory of such systems indicates solutions will be consist of either two shocks, a composite

shock-rarefaction, or a singular shock, depending on the details of the precursor model. Changing the form of the particle settling velocity eliminates the need for un-physical singular shock solutions, and the resulting system appears to always have a classical weak solution of either two shocks or a rarefaction-shock. The double-shock solutions have the same structure as the particle-rich ridge observed in experiments.

In chapter 4 a linear stability analysis of the advancing film shows a long-wave instability, as in the fluid case, corresponding to the observed finger-like deformations of the contact line. Numerical studies indicate two-dimensional problem requires additional regularization in order to be well-posed, and a simple model is presented for such a regularization due to shear-induced diffusion. The stability calculation for this regularized system shows that particle settling, and the associated particle-rich ridge, has a mild stabilizing effect on the contact line and shifts the most unstable mode to slightly longer wavelengths. This result is in qualitative agreement with Zhou et al.'s observation that the instability is somewhat suppressed by the formation of a ridge.

Chapter 5 considers a more general model for particle-laden films, allowing the particle concentration to vary with depth. This model assumes that the concentration reaches a steady state in which vertical settling is balanced by shear-induced migration. Depending on the overall concentration and the incli-nation angle, this balance can result in higher concentrations at the top or the bottom. This distinction determines whether particles move on average faster or slower than the liquid, which in turn probably determines whether particles settle out of the flow or accumulate in a ridge. A straightforward application to a one-dimensional flow appears computationally feasible and could quantify this statement. Predictions of the settling behavior are consistent with the ex-

perimental phase diagram in [ZDB05]. A drawback of this model however is that the concentration may not always be in equilibrium, particularly in regions near a shock. Numerical simulation of the non-equilibrium version of this model represents a more challenging problem for further study.

References

[Bag54]   R. A. Bagnold. "Experiments on a Gravity-Free Dispersion of Large Solid Spheres in a Newtonian Fluid under Shear." *Proc. Royal Soc. London A*, **225**(1160):49–63, 1954.

[Bat72]   G. K. Batchelor. "Sedimentation in a dilute dispersion of spheres." *J. Fluid Mech.*, **52**:245–268, 1972.

[BB88]   John F. Brady and Georges Bossis. "Stokesian Dynamics." *Ann. Rev. Fluid Mech.*, **20**:111–157, 1988.

[BB97]   Andrea L. Bertozzi and Michael P. Brenner. "Linear stability and transient growth in driven contact lines." *Phys. Fluids*, **9**(3), 1997.

[BG72]   G. K. Batchelor and J. T. Green. "The determination of the bulk stress in a suspension of spherical particles to order c^2." *J. Fluid Mech.*, **56**:401–427, 1972.

[BGO82]   R. Buscall, J. W. Goodwin, R. H. Ottewill, and T. F. Tadros. "The settling of particles through Newtonian and non-Newtonian media." *J. Colloid Interface Sci.*, **85**(1):78–86, 1982.

[BLS95]   W. H. Boersma, J Laven, and H N Stein. "Computer Simulations of Shear Thickening of Concentrated Dispersions." *J. Rheology*, **39**(5):841–860, 1995.

[BM73]   E. Barnea and J. Mizrahi. "A generalized approach to the fluid-dynamics of particulate systems, part 1: General correlation for fluidization and sedimentation." *Chem. Eng. J.*, **5**:171–189, 1973.

[BMS99]   A. L. Bertozzi, A. Münch, and M. Shearer. "Undercompressive shocks in thin film flows." *Phys. D*, **134**:431–464, 1999.

[BSB05]   Mark Bowen, Jeanman Sur, Andrea L. Bertozzi, and Robert P. Behringer. "Nonlinear dynamics of two-dimensional undercompressive shocks." *Physica D. Nonlinear Phenomena*, **209**(1-4):36–48, 2005.

[CBH06]   B. P. Cook, A. L. Bertozzi, and A. E. Hosoi. "Shock solutions for particle-laden thin films." *SIAM J. Appl. Math.*, 2006. submitted.

[CL85]   R. E. Caflisch and J. H. C. Luke. "Variance in the sedimentation speed of a suspension." *Phys. Fluids*, **28**(259), 1985.

[CP94]   C. Y. Chang and R. L. Powell. "The Rheology of Bimodal Hard-Sphere Dispersions." *Phys. Fluids*, **6**:1628–1636, 1994.

[de 85]   P. G. de Gennes. "Wetting: Statics and Dynamics." *Reviews of Modern Physics*, **57**(3), 1985.

[de 92]   John R. de Bruyn. "Growth of fingers at a driven three-phase contact line." *Phys. Rev. A*, **46**:R4500–R4503, 1992.

[Ein06]   Albert Einstein. "Calculation of the viscosity-coefficient of a liquid in which a large number of small spheres are suspended." *Ann. Physik*, 1906.

[ESR00]   M. H. Eres, L. W. Schwartz, and R. V. Roy. "Fingering phenomena for driven coating films." *Phys. Fluids*, **12**(6):1278–1295, 2000.

[FB00]   David R. Foss and John F. Brady. "Stucture, diffusion, and rheology of Brownian Suspensions by Stokesian Dynamics simulation." *F. Fluid Mech.*, **407**:167–200, 2000.

[FMB02]   Z. W. Fang, A. A. Mammoli, J. F. Brady, M. S. Ingber, L. A. Mondy, and A. L. Graham. "Flow-aligned tensor models for suspension flows." *Int. J. Multiphase Flow*, **28**(1):137–166, 2002.

[GA77]   J. Garside and M. R. Al-Dibouni. "Velocity-voidage relationship for fluidization and sedimentation in solid-liquid systems." *Ind. Eng. Chem. Process Des. Dev.*, **16**:206–214, 1977.

[GH91]   Ralph Goodwin and G. M. Homsy. "Viscous flow down a slope in the vicinity of a contact line." *Phys. Fluids A*, **3**:515–528, 1991.

[Gre78]   H. P. Greenspan. "On the motion of a small viscous droplet that wets a surface." *J. Fluid Mech.*, **84**:125–143, 1978.

[HB65]   John Happel and Howard Brenner. *Low Reynolds number hydrodynamics, with special applications to particulate media.* Prentice-Hall, 1965.

[HS71]   Chun Huh and L. E. Scriven. "Hydrodynamic model of steady movement of a solid/liquid/fluid contact line." *J. Colloid Interface Sci.*, **35**(1):85–101, 1971.

[Hup82]   H. E. Huppert. "Flow and instability of a viscous current down a slope." *Nature*, **300**, 1982.

[IM98]   M. P. Ida and M. J. Miksis. "The Dynamics of Thin Films I: General Theory." *SIAM J. Appl. Math.*, **58**(2):456–473, 1998.

[IVC98]   A. Indekina, I. Veretennikov, and H.-C. Chang. "Front dynamics and fingering of a driven contact line." *J. Fluid Mech.*, **373**:81, 1998.

[Jd92]   John M. Jerrett and John R. de Bruyn. "FIngering instability of a gravitationally driven contact line." *Phys. Fluids A*, **4**:234–242, 1992.

[JFP06]   P. Jop, Y. Forterre, and O. Pouliquen. "A constitutive law for dense granular flows." *Nature*, **441**:727–730, 2006.

[JG92]   O. E. Jensen and J. B. Grotberg. "Insoluble surfactant spreading on a thin viscous film - shock evolution and film rupture." *J. Fluid Mech.*, **240**:259–288, 1992.

[Kal00]   S. Kalliadasis. "Nonlinear instability of a contact line driven by gravity." *J. Fluid Mech.*, **413**:355–378, 2000.

[KD01]   L. Kondic and J. Diez. "Pattern formation in the flow of thin films down an incline: Constant flux configuration." *Phys. Fluids*, **13**:3168, 2001.

[KK90]   Herbert C. Kranzer and Barbara Lee Keyfitz. "A strictly hyperbolic system of conservation laws admitting singular shocks." *IMA Volumes in Mathematics and its Applications*, pp. 107–125, 1990.

[KK95]   Barbara Lee Keyfitz and Herbert C. Kranzer. "Spaces of weighted measures for conservation laws with singular shock solutions." *J. Differential Equations*, **118**(2):420–451, 1995.

[Kri72]   Irvin M. Krieger. "Rheology of Monodisperse Latices." *Advances in Colloid and Interface Science*, **3**:111–136, 1972.

[Kyn52]   G. J. Kynch. "A Theory of Sedimentation." *Trans. Faraday Soc.*, **48**:166–176, 1952.

[LA86]   David Leighton and Andreas Acrivos. "Viscous Resuspension." *Chemical Engineering Science*, **41**(6), 1986.

[LA87]   David Leighton and Andreas Acrivos. "The shear-induced migration of particles in concentrated suspensions." *J. Fluid Mech.*, **181**, 1987.

[Lax73]   Peter D. Lax. *Hyperbolic systems of conservation laws and mathematical theory of shock waves*, volume 11 of *CBMS-NSF Regional Conference Series in Applied Mathematics*. SIAM, 1973.

[Lei85]   D. Leighton. *The shear induced migration of particulates in concentrated suspensions.* PhD thesis, Stanford Univ., Stanford, California, 1985.

[LHM97]   L. Léger, H. Hervet, G. Massey, and E. Durliat. "Wall slip in polymer melts." *J. Phys.: Condens. Matter*, **9**:7719–7740, 1997.

[Liu74]   Tai-Ping Liu. "The Riemann problem for general 2×2 conservation laws." *Trans. Amer. Math. Soc.*, **199**:898–112, 1974.

[Liu75]   Tai-Ping Liu. "Riemann problem for general systems of conservation laws." *J. Differential Equations*, **18**(1):218–234, 1975.

[LL71]   V. Ludviksson and E. N. Lightfoot. "The dynamics of thin liquid films in the presence of surface-tension gradients." *Am. Inst. Chem. Engrs. J.*, **17**(5):1166–1173, 1971.

[LS06]   R. Levy and M. Shearer. "The Motion of a thin liquid film driven by surfactant and gravity." *SIAM J. Appl. Math.*, **66**(5):1688–1609, 2006.

[MB98]   J. F. Morris and J. F. Brady. "Pressure-driven flow of a suspension: buoyancy effects." *Int. J. Multiphase Flow*, **24**:105–130, 1998.

[NB94]   Prabhu R. Nott and John F. Brady. "Pressure-driven flow of suspensions: simulation and theory." *J. Fluid Mech.*, **275**, 1994.

[ODB97]   Alexander Oron, Stephen H. Davis, and S. George Bankoff. "Long-scale evolution of thin liquid films." *Rev. Modern Phys.*, **69**(3):931–980, 1997.

[Ole63]   O. A. Oleinik. "Discontinuous Solutions of nonlinear differential equations." *Amer. Math. Soc. Transl.*, **26**(2):95–172, 1963.

[PAB92]   R. J. Phillips, R. C. Armstrong, R. A. Brown, A. L. Graham, and J. R. Abbott. "A constitutive equatioin for concentrated suspensions that accounts for shear-induced particle migration." *Phys. Fluids A*, **4**(1):30–40, 1992.

[PDS97]   O. Pouliquen, J. Delour, and S. B. Savage. "Fingering in granular flow." *Nature*, **386**(6627):816–817, 1997.

[Pou99]   O. Pouliquen. "Scaling laws in granular flows down rough inclined planes." *Phys. Fluids*, **11**(3):542–548, 1999.

[RZ54]   J. F. Richardson and W. N. Zaki. "Sedimentation and Fluidization: Part I." *Trans. Inst. Chem. Eng.*, **32**:35–53, 1954.

[Sat95]   T. Sato. "Rheology of suspensions." *J. Coat. Technol.*, **67**(847):69–79, 1995.

[SAZ90]   U. Schaflinger, A. Acrivos, and K. Zhang. "Viscous resuspension of a sediment within a laminar and stratified flow." *Int. J. Multiphase Flow*, **16**(4):567–578, 1990.

[SB01]   A. Seirou and J. F. Brady. "Accelerated Stokesian Dynamics simulations." *J. Fluid Mech.*, **448**:115–146, 2001.

[SB02]   A. Sierou and J. F. Brady. "Rheology and Microstructure in concentrated noncolloidal suspensions." *J. Rheology*, **46**(5):1031–1056, 2002.

[SD85]   N. Silvi and E. B. Dussan V. "On the rewetting of an inclined solid surface by a liquid." *Phys. Fluids*, **28**:5–7, 1985.

[Sev07]   Michael Sever. "Distribution solutions of nonlinear systems of conservation laws." *Mem. Amer. Math. Soc.*, 2007. to appear.

[SH95]   M. A. Spaid and G. M. Homsy. "Stability of Newtonian and viscoelastic dynamic contact lines." *Phys. Fluids*, **8**(2):460–478, 1995.

[SP05]   Jonathan J. Stickel and Robert L. Powell. "Fluid mechanics and rheology of dense suspensions." *Ann. Rev. Fluid Mech.*, **37**:129–149, 2005.

[THS89]   S. M. Troian, E. Herbolzheimer, S. A. Safran, and J. F. Joanny. "Fingering Instabilities of Driven Spreading Films." *Europhys. Lett.*, **10**(1), 1989.

[TM05]   Brian D. Timberlake and Jeffrey F. Morris. "Particle Migration and Free-Surface Topography in Inclined Plane Flow of a Suspension." *J. Fluid Mech.*, **538**, 2005.

[Ung93]   Marius Ungarish. *Hydrodynamics of Suspensions*, chapter 2: Physico-Mathematical Formulation, pp. 7–36. Springer-Verlag, 1993.

[WCM04]   M. R. E. Warner, R. V. Craster, and O. K. Matar. "Fingering phenomena associated with insoluble surfactant spreading on thin liquid films." *J. Fluid Mech.*, **510**:169–200, 2004.

[XP03]   L. Xianfan and C. Pozrikidis. "Film flow of a suspension down an inclined plane." *Phil. Trans. R. Soc. Lond.*, **361**:847, 2003.

[You05]   Thomas Young. "An Essay on the Cohesion of Fluids." *Philos. Trans. Royal Soc. London*, **95**:65–87, 1805.

[ZDB05]   Junjie Zhou, B. Dupuy, A.L. Bertozzi, and A. E. Hosoi. "Theory for shock dynamics in particle-laden thin films." *Phys. Rev. Lett.*, **94**, 2005.

[Zho04]   Junjie Zhou. *"Reduced Model for Particle Laden Flow."*. Master's thesis, Massachucetts Institute of Technology, 2004.